

Salient Object Detection in the Deep Learning Era: An In-depth Survey

Wenguan Wang, *Member, IEEE*, Qiuxia Lai, Huazhu Fu, *Senior Member, IEEE*, Jianbing Shen, *Senior Member, IEEE*, Haibin Ling, and Ruigang Yang, *Senior Member, IEEE*

Abstract—As an essential problem in computer vision, salient object detection (SOD) has attracted an increasing amount of research effort over the years. Recent advances in SOD are dominantly led by deep learning-based solutions (named deep SODs). To facilitate the in-depth understanding of deep SODs, in this paper, we provide a comprehensive survey covering various aspects ranging from algorithm taxonomy to unsolved open issues. In particular, we first review deep SOD algorithms from different perspectives, including network architecture, level of supervision, learning paradigm, and object/instance level detection. Following that, we summarize and analyze existing SOD datasets and evaluation metrics. Then, we benchmark a large group of representative SOD models, and provide detailed analyses of the comparison results. Moreover, we study the performance of SOD algorithms under different attributes, which have been hardly explored previously, by constructing a novel SOD dataset with rich attribute annotations covering various salient object types, challenging factors, and scene categories. We further analyze, for the first time in the field, the robustness of SOD models w.r.t. random input perturbations and adversarial attacks. We also look into the generalization and hardness of existing SOD datasets. Finally, we discuss several open issues of SOD and outline future research directions. All the saliency prediction maps, our constructed dataset with annotations, and codes for evaluation are publicly available at <https://github.com/wenguanwang/SODsurvey>.

Index Terms—Salient Object Detection, Deep Learning, Benchmark, Image Saliency.

1 INTRODUCTION

SALIENT object detection (SOD) aims at highlighting visually salient object regions in images, which is driven by and applied to a wide spectrum of object-level applications in various areas. In computer vision, representative applications include image understanding [1], [2], image captioning [3]–[5], object detection [6], [7], un-supervised video object segmentation [8], [9], semantic segmentation [10]–[12], person re-identification [13], [14], video summarization [15], [16], *etc.* In computer graphics, SOD plays an essential role in various tasks like non-photo-realist rendering [17], [18], automatic image cropping [19], image retargeting [20], [21], *etc.* Exemplary applications in robotics, like human-robot interaction [22], [23], and object discovery [24], [25], also benefit from SOD for better scene/object understanding.

Different from fixation prediction (FP), which is originated from cognitive and psychology research communities to investigate the human attention mechanism by predicting eye fixation positions in visual scenes, SOD is inspired by FP and aims at highlighting the whole attentive ob-

jects/regions. Significant improvement for SOD has been witnessed in recent years with the renaissance of deep learning techniques, thanks to the powerful representation learning methods. Since the first introduction in 2015 [26]–[28], deep learning-based SOD (or *deep SOD*) algorithms have soon shown superior performance over traditional solutions, and kept residing the top of various benchmarking leaderboards. On the other hand, hundreds of research papers have been produced on deep SOD, making it non-trivial for effectively understanding the state-of-the-arts.

This paper provides a comprehensive and in-depth survey of SOD in the deep learning era. In addition to taxonomically reviewing existing deep SOD methods, it provides in-depth analyses of representative datasets and evaluation metrics, investigates crucial but largely under-explored issues such as robustness and transferability of deep SOD models, strength and weakness with certain scenarios (*i.e.*, scene/salient object categories, challenging factors), generalizability and hardness of SOD datasets. All the saliency maps used for benchmarking, our constructed dataset with annotations, and codes for evaluation are publicly available at <https://github.com/wenguanwang/SODsurvey>.

1.1 History and Scope

Human beings are able to quickly allocate attentions on important regions in visual scenes. Understanding and modeling such an astonishing ability, *i.e.*, visual attention or visual saliency, is a fundamental research problem in psychology, neurobiology, cognitive science, and computer vision. There are two categories of computational models for visual saliency, namely FP and SOD. FP originated from cognitive and psychology communities [50]–[52], which is to predict the human fixation points when observing a scene.

- W. Wang is with ETH Zurich, Switzerland. (Email: wenguanwang.ai@gmail.com)
- Q. Lai is with the Department of Computer Science and Engineering, the Chinese University of Hong Kong, Hong Kong, China. (Email: qxilai@cse.cuhk.edu.hk)
- H. Fu is with Inception Institute of Artificial Intelligence, UAE. (Email: hzfu@ieee.org)
- J. Shen is with Beijing Laboratory of Intelligent Information Technology, School of Computer Science, Beijing Institute of Technology, China. (Email: shenjianbing@bit.edu.cn)
- H. Ling is with the Department of Computer and Information Sciences, Temple University, Philadelphia, PA, USA. (Email: hbling@temple.edu)
- R. Yang is with the University of Kentucky, Lexington, KY 40507. (Email: ryang@cs.uky.edu)
- First two authors contribute equally.
- Corresponding author: Jianbing Shen

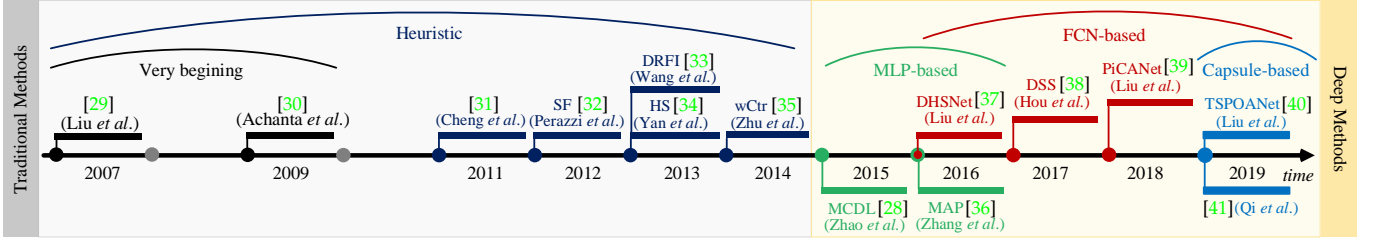


Fig. 1. A brief chronology of SOD. The very first SOD models date back to the work of Liu *et al.* [29] and Achanta *et al.* [30]. The first incorporation of deep learning techniques in SOD models is from 2015. Listed methods are milestones, which are typically highly cited. See §1.1 for more details.

TABLE 1

Summary of previous reviews. For each work, the publication information and coverage are provided. See §1.2 for more detailed descriptions.

Title	Year	Venue	Description
State-of-the-Art in Visual Attention Modeling [42]	2013	TPAMI	This paper reviews visual attention (<i>i.e.</i> fixation prediction) models before 2013.
Salient Object Detection: A Benchmark [43]	2015	TIP	This paper benchmarks 29 heuristic SOD models and 10 FP methods over 7 datasets.
Attentive Systems: A Survey [44]	2017	IJCV	This paper reviews applications that utilize visual saliency cues.
A Review of Co-Saliency Detection Algorithms: Fundamentals, Applications, and Challenges [45]	2018	TIST	This paper reviews the fundamentals, challenges, and applications of co-saliency detection.
Review of Visual Saliency Detection with Comprehensive Information [46]	2018	TCSVT	This paper reviews RGB-D SOD, co-saliency detection and video SOD.
Advanced Deep-Learning Techniques for Salient and Category-Specific Object Detection: A survey [47]	2018	SPM	This paper reviews several sub-directions of object detection, namely objectness detection, SOD and category-specific object detection.
Saliency prediction in the deep learning era: Successes and limitations [48]	2019	TPAMI	This paper reviews image and video fixation prediction models and analyzes specific questions.
Salient Object Detection: A Survey [49]	2019	CVM	This paper reviews 65 heuristic and 21 deep SOD models till 2017 and discusses closely related areas like object detection, fixation prediction, segmentation, <i>etc.</i>

The history of SOD is relatively short and can be traced back to [29] and [30]. The rise of SOD is driven by the wide range of object-level computer vision applications. Most of early, **non-deep SOD models** [35], [53] rely on low-level features and certain heuristics (*e.g.*, *color contrast* [31], *background prior* [54]). To obtain uniformly highlighted salient objects and clear object boundaries, an over-segmentation process that generates regions [55], super-pixels [56], [57], or object proposals [58] is often integrated into above models. Please see [43] for a comprehensive overview.

With the compelling success of deep learning technologies in computer vision, more and more **deep SOD methods** have been springing up since 2015. Earlier deep SOD models typically utilize multi-layer perceptron (MLP) classifiers to predict the saliency score of deep features extracted from each image processing unit [26]–[28]. Later, a more effective and efficient form, *i.e.*, fully convolutional network (FCN)-based network, becomes the mainstream of SOD architectures. Some recent arts [40], [41] also introduce Capsule [59] into SOD for addressing object property modeling comprehensively. A brief chronology of SOD is shown in Fig. 1.

Scope of the survey. Despite having a short history, research in deep SOD has produced hundreds of papers, making it impractical (and fortunately unnecessary) to review all of them. Instead, we comprehensively select influential papers published in prestigious journals and conferences. This survey mainly focuses on the major progress in the last five years, but for completeness and better readability, some early related works are also included. It is worth noting that we restrict this survey to *single image SOD* methods, and leave RGB-D SOD, co-saliency detection, video SOD, FP, social gaze prediction, *etc.*, as separate topics.

1.2 Related Previous Reviews and Surveys

Table 1 lists existing surveys that are related to ours. Among them, Borji *et al.* [43] review SOD methods preceding 2015,

thus do not refer to recent deep learning-based solutions. Zhang *et al.* [45] review methods for co-saliency detection, *i.e.*, detecting common salient objects from multiple relevant images. Cong *et al.* [46] review several extended SOD tasks including RGB-D SOD, co-saliency detection and video SOD. Han *et al.* [47] look into the sub-directions of object detection, and conclude the recent progress in objectness detection, SOD, and category-specific object detection. Borji *et al.* summarize both heuristic [42] and deep models [48] for FP. Nguyen *et al.* [44] focus on categorizing the applications of visual saliency (including both SOD and FP) in different areas. A recently published survey [49] covers both traditional non-deep methods and deep ones till 2017, and discusses the relation w.r.t. several other closely-related research areas such as special-purpose object detection and segmentation.

Different from previous SOD surveys that focus on earlier non-deep learning SOD methods [43], other related fields [42], [46]–[48], practical applications [44] or limited number of deep SOD models [49], this work systematically and comprehensively review recent advances in the field. It is featured by in-depth analysis and discussion in various aspects, many of which, to the best of our knowledge, are the first time in this field. In particular, we summarize and feature existing deep SOD methods from a comprehensive view based on several proposed taxonomies (§2), review datasets (§3) and evaluation metrics (§4) with their pros and cons, gain a deeper understanding of SOD models through attribute-based evaluation (§5.3), discuss on the influence of input perturbation (§5.4), analyze the robustness of deep SOD models w.r.t. adversarial attacks (§5.5), study the generalization and hardness of existing SOD datasets (§5.6), and offer insights for essential open issues, challenges, and future directions (§6). We expect our survey to provide novel insights and inspiration for facilitating the understanding of deep SOD, and to foster research on the raised open issues such as adversarial attacks to SOD.

TABLE 2
Taxonomies and representative publications of deep SOD methods. See §2 for more detailed descriptions.

Category			Publications	
Network Architectures (§2.1)	Multi-layer perceptron (MLP)-based	1) Super-pixel/patch-based 2) Object proposal based	[28], [60], [26], [61] [27], [36], [62]	
	Fully convolutional network (FCN)-based	1) Single-stream 2) Multi-stream 3) Side-fusion 4) Bottom-up/top-down 5) Branched	[63], [64], [65], [66], [67], [68], [69] [70], [71], [72], [73], [74] [38], [75], [76], [77], [78], [79], [80], [81], [82] [37], [83], [84], [85], [86], [87], [39], [88], [89], [90], [91], [92], [93], [94], [95] [96], [97], [98], [99], [100], [101], [102], [103]	
		Hybrid network-based	[104], [105]	
		Capsule-based	[40], [41]	
		Level of Supervision (§2.2)	Fully-supervised	All others
	Un-/Weakly-supervised	1) Category-level 2) Pseudo pixel-level	[97], [68], [69], [81] [83], [98], [67], [99]	
Learning Paradigm (§2.3)		Single-task learning (STL)	All others	
Mingle-task learning (MTL)		1) Salient object subitizing 2) Fixation prediction 3) Image classification 4) Semantic segmentation 5) Contour/edge detection 6) Image captioning	[36], [77], [79] [96], [87] [97], [98] [63], [103] [75], [99], [89], [91], [92], [93], [101], [82], [102] [100]	
		Object-/Instance-Level (§2.4)	Object-level	All others
		Instance-level	[36], [70]	

1.3 Our Contributions

Our contributions in this paper are summarized as follows:

- 1) **A systematic review of deep SOD models from various perspectives.** We categorize and summarize existing deep SOD models according to network architecture, level of supervision, learning paradigm, *etc.* The proposed taxonomies aim to help researchers with a deeper understanding of the key features of deep SOD models.
- 2) **An attribute-based performance evaluation of SOD models.** We compile a hybrid dataset and provide annotated attributes about object categories, scene categories, and challenging factors. By evaluating several representative SOD models on it, the results uncover strengths and weaknesses of deep and non-deep approaches, opening up promising directions for future efforts.
- 3) **An analysis of the robustness of SOD models against general input perturbations.** To study the robustness of SOD models, we investigate the effects of various perturbations on final performance of deep and non-deep SOD models. Some results are somewhat unexpected.
- 4) **The first known adversarial attack analysis on SOD models.** We further examine robustness of SOD models against intentionally designed perturbations, *i.e.*, adversarial attack. The specially designed attacks and evaluations could serve as baselines for future study of the robustness and transferability of deep SOD models.
- 5) **Cross-dataset generalization study.** To in-depth analyze the generalization and difficulty of existing SOD datasets, we conduct a cross-dataset generalization study that quantitatively reveals the dataset bias.
- 6) **Overview of open issues and future directions.** We thoroughly look over several essential issues (*i.e.*, model design, dataset collection, *etc.*), which shed light on potential directions for future research.

These contributions altogether bring an exhaustive, up-to-date, and in-depth survey, and differentiate it from previous review papers significantly.

The rest of the paper is organized as follows. §2 explains the proposed taxonomies, each accompanied with

one or two most representative models. §3 examines the most notable SOD datasets, whereas §4 describes several widely used SOD metrics. §5 benchmarks several deep SOD models and provides in-depth analyses. §6 provides further discussions and presents open issues and future research directions of the field. Finally, §7 concludes the paper.

2 DEEP LEARNING BASED SOD MODELS

Before reviewing in details recent deep SOD models, we first give a common formulation of the image-based SOD problem. Given an input image $I \in \mathbb{R}^{W \times H \times 3}$ of size $W \times H$, an SOD model f maps the input image I to a continuous saliency map $S = f(I) \in [0, 1]^{W \times H}$. For learning-based SOD, the model f is learned through a set of training samples. Given a set of static images $\mathcal{I} = \{I_n \in \mathbb{R}^{W \times H \times 3}\}_n$ and corresponding binary SOD ground-truth masks $\mathcal{G} = \{G_n \in \{0, 1\}^{W \times H}\}_n$, the goal of learning is to find $f \in \mathcal{F}$ that minimizes the prediction error, *i.e.*, $\sum_n \ell(S_n, G_n)$, where ℓ is a certain distance measure (*e.g.*, defined in §4), $S_n = f(I_n)$, and \mathcal{F} is the set of potential mapping functions. Deep SOD methods typically model f through modern deep learning techniques, as will be reviewed in this section. The ground-truths \mathcal{G} can be collected by different methodologies, *i.e.*, direct human-annotation or eye-fixation-guided labeling, and may have different formats, *i.e.*, pixel-wise or bounding-box level annotations, which will be discussed in §3.

In Table 2, we categorize recent deep SOD models according to four taxonomies, considering typical *network architecture* (§2.1), *level of supervision* (§2.2), *learning paradigm* (§2.3), and being *object-level* or *instance-level* (§2.4). In the following, each category is elaborated and exemplified by one or two most representative models. Table 3 summarizes essential characteristics of recent SOD models.

2.1 Representative Network Architectures for SOD

Based on the primary network architectures adopted, we classify deep SOD models into four categories, namely *MLP-based* (§2.1.1), *FCN-based* (§2.1.2), *hybrid network-based* (§2.1.3) and *Capsule-based* (§2.1.4).

TABLE 3

Summary of essential characteristics for popular SOD methods. Here, '#Training' is the number of training images, and 'CRF' denotes whether the predictions are post-processed by Conditional Random Field [106]. See §2 for more detailed descriptions.

	Methods	Publ.	Architecture	Backbone	Level of Supervision	Learning Paradigm	Obj.-/Inst.-Level SOD	Training Dataset	#Training	CRF
2015	SuperCNN [61]	IJCV	MLP+super-pixel	-	Fully-Sup.	STL	Object	ECSSD [55]	800	
	MCDL [28]	CVPR	MLP+super-pixel	GoogleNet	Fully-Sup.	STL	Object	MSRA10K [107]	8,000	
	LEGS [27]	CVPR	MLP+segment	-	Fully-Sup.	STL	Object	MSRA-B [29]+PASCAL-S [108]	3,000+340	
	MDF [60]	CVPR	MLP+segment	-	Fully-Sup.	STL	Object	MSRA-B [29]	2,500	
2016	ELD [60]	CVPR	MLP+super-pixel	VGGNet	Fully-Sup.	STL	Object	MSRA10K [107]	~9,000	
	DHSNet [37]	CVPR	FCN	VGGNet	Fully-Sup.	STL	Object	MSRA10K [107]+DUT-OMRON [56]	6,000+3,500	
	DCL [104]	CVPR	FCN	VGGNet	Fully-Sup.	STL	Object	MSRA-B [29]	2,500	✓
	RACDNN [64]	CVPR	FCN	VGGNet	Fully-Sup.	STL	Object	DUT-OMRON [56]+NJU2000 [109]+RGBD [110]	10,565	
	SU [96]	CVPR	FCN	VGGNet	Fully-Sup.	MTL	Object	MSRA10K [107]+SALICON [111]	10,000+15,000	✓
	MAP [36]	CVPR	MLP+obj. prop.	VGGNet	Fully-Sup.	MTL	Instance	SOS [112]	~5,500	
	SSD [62]	ECCV	MLP+obj. prop.	AlexNet	Fully-Sup.	STL	Object	MSRA-B [29]	2,500	
	CRPSD [105]	ECCV	FCN	VGGNet	Fully-Sup.	STL	Object	MSRA10K [107]	10,000	
2017	RFCN [63]	ECCV	FCN	VGGNet	Fully-Sup.	MTL	Object	PASCAL VOC 2010 [113]+MSRA10K [107]	10,103+10,000	
	MSRNet [70]	CVPR	FCN	VGGNet	Fully-Sup.	STL	Instance	MSRA-B [29]+HKU-IS [26] (+ILSO [70])	2,500+2,500 (+500)	✓
	DSS [38]	CVPR	FCN	VGGNet	Fully-Sup.	STL	Object	MSRA-B [29]+HKU-IS [26]	2,500	✓
	WSS [97]	CVPR	FCN	VGGNet	Weakly-Sup.	MTL	Object	ImageNet [114]	456k	✓
	DLS [65]	CVPR	FCN	VGGNet	Fully-Sup.	STL	Object	MSRA10K [107]	10,000	
	NLDF [75]	CVPR	FCN	VGGNet	Fully-Sup.	MTL	Object	MSRA-B [29]	2,500	✓
	DSOS [77]	ICCV	FCN	VGGNet	Fully-Sup.	MTL	Object	SOS [112]	6,900	
	Amulet [76]	ICCV	FCN	VGGNet	Fully-Sup.	STL	Object	MSRA10K [107]	10,000	
	FSN [72]	ICCV	FCN	VGGNet	Fully-Sup.	STL	Object	MSRA10K [107]	10,000	
	SBF [83]	ICCV	FCN	VGGNet	Un-Sup.	STL	Object	MSRA10K [107]	10,000	
	SRM [71]	ICCV	FCN	ResNet	Fully-Sup.	STL	Object	DUTS [97]	10,553	
	UCF [66]	ICCV	FCN	VGGNet	Fully-Sup.	STL	Object	MSRA10K [107]	10,000	
2018	RADF [78]	AAAI	FCN	VGGNet	Fully-Sup.	STL	Object	MSRA10K [107]	10,000	✓
	ASMO [98]	AAAI	FCN	ResNet101	Weakly-Sup.	MTL	Object	MS COCO [115]+MSRA-B [29]+HKU-IS [26]	82,783+2,500+2,500	✓
	LICNN [68]	AAAI	FCN	VGGNet	Weakly-Sup.	STL	Object	ImageNet [114]	456k	
	BDMP [84]	CVPR	FCN	VGGNet	Fully-Sup.	STL	Object	DUTS [97]	10,553	
	DUS [67]	CVPR	FCN	ResNet101	Un-Sup.	MTL	Object	MSRA-B [29]	2,500	
	DGRL [85]	CVPR	FCN	ResNet50	Fully-Sup.	STL	Object	DUTS [97]	10,553	
	PAGR [86]	CVPR	FCN	VGGNet19	Fully-Sup.	STL	Object	DUTS [97]	10,553	
	RSDNet [79]	CVPR	FCN	ResNet101	Fully-Sup.	MTL	Object	PASCAL-S [108]	425	
	ASNet [87]	CVPR	FCN	VGGNet	Fully-Sup.	MTL	Object	SALICON [111]+MSRA10K [107]+DUT-OMRON [56]	15,000+10,000+5,168	
	PiCANet [39]	CVPR	FCN	VGGNet/ResNet50	Fully-Sup.	STL	Object	DUTS [97]	10,553	✓
	C2S-Net [99]	ECCV	FCN	VGGNet	Weakly-Sup.	MTL	Object	MSRA10K [107]+Web	10,000+20,000	
	RAS [88]	ECCV	FCN	VGGNet	Fully-Sup.	STL	Object	MSRA-B [29]	2,500	
2019	SuperVAE [69]	AAAI	FCN	N/A	Un-Sup.	STL	Object	N/A	N/A	
	DEF [74]	AAAI	FCN	ResNet101	Fully-Sup.	STL	Object	DUTS [97]	10,553	
	AFNet [89]	CVPR	FCN	VGGNet16	Fully-Sup.	MTL	Object	DUTS [97]	10,553	
	BASNet [90]	CVPR	FCN	ResNet-34	Fully-Sup.	STL	Object	DUTS [97]	10,553	
	CapSal [100]	CVPR	FCN	ResNet101	Fully-Sup.	MTL	Object	COCO-CapSal [100]/DUTS [97]	5,265/10,553	
	CPD-R [80]	CVPR	FCN	ResNet50	Fully-Sup.	STL	Object	DUTS [97]	10,553	
	MLSLNet [91]	CVPR	FCN	VGG16	Fully-Sup.	MTL	Object	DUTS [97]	10,553	
	†MWS [81]	CVPR	FCN	N/A	Weakly-Sup.	STL	Object	ImageNet DET [114]+MS COCO [115] +ImageNet [116]+DUTS [97]	456k+82,783 +300,000+10,553	
	PAGE-Net [92]	CVPR	FCN	VGGNet16	Fully-Sup.	MTL	Object	MSRA10K [107]	10,000	✓
	PS [94]	CVPR	FCN	ResNet50	Fully-Sup.	STL	Object	MSRA10K [107]	10,000	✓
	PoolNet [93]	CVPR	FCN	ResNet50	Fully-Sup.	STL/MTL	Object	DUTS [97]	10,553	
	BANet [101]	ICCV	FCN	ResNet50	Fully-Sup.	MTL	Object	DUTS [97]	10,553	
	EGNet [82]	ICCV	FCN	VGGNet/ResNet	Fully-Sup.	MTL	Object	DUTS [97]	10,553	
	HRSOD [73]	ICCV	FCN	VGGNet	Fully-Sup.	STL	Object	DUTS [97]/HRSOD [73]+DUTS [97]	10,553/12,163	
	JDFPR [95]	ICCV	FCN	VGG	Fully-Sup.	STL	Object	MSRA-B [29]	2,500	✓
	SCRN [102]	ICCV	FCN	ResNet50	Fully-Sup.	MTL	Object	DUTS [97]	10,553	
	SSNet [103]	ICCV	FCN	Desenet169	Fully-Sup.	MTL	Object	PASCAL VOC 2012 [113]+DUTS [97]	1,464+10,553	✓
	TSPONet [40]	ICCV	Capsule	FLNet	Fully-Sup.	STL	Object	DUTS [97]	10,553	

2.1.1 Multi-Layer Perceptron (MLP)-based Methods

MLP-based methods leverage image subunits (*i.e.*, *super-pixels/patches* [28], [60], [61], and generic *object proposals* [26], [27], [36], [62]) as processing units. They fed deep features extracted from the subunits into an MLP-classifier for saliency score prediction (Fig. 2(a)).

1) Super-pixel/patch-based methods use regular (patch) or nearly-regular (super-pixel) image decomposition.

- **MCDL [28]** uses two pathways for extracting local and global context from two super-pixel-centered windows of different sizes. The global and local feature vectors are fed into an MLP for classifying background and saliency.

2) Object proposal-based methods leverage object proposals [26], [27] or bounding-boxes [36], [62] as basic processing units in order to better encode object information.

- **MAP [36]** uses a CNN model to generate a set of scored bounding boxes, then selects an optimized compact subset of bounding boxes as the salient objects.

Though MLP-based SOD methods outperformed non-deep counterparts greatly, they cannot fully leverage essen-

tial spatial information and are quite time-consuming, as they need to process all visual subunits one-by-one.

2.1.2 Fully Convolutional Network (FCN)-based Methods

To address the limitations of MLP-based methods, recent solutions adopt FCN architecture [117], leading to end-to-end spatial saliency representation learning and fast saliency prediction, only within one single feed-forward process. FCN-based methods are the dominant in the filed. Typical architectures can be further classified as: *single-stream network*, *multi-stream network*, *side-fusion network*, *bottom-up/top-down network*, and *branched network*.

1) Single-stream network is the most standard architecture, which has a stack of convolution layers, intermediated by pooling and non-linear activation operations (see Fig. 2(b)). It takes a whole image as input, and directly outputs a pixel-wise probabilistic map highlighting salient objects.

- **UCF [66]** makes use of an encoder-decoder network architecture for finer-resolution saliency prediction. It incorporates a reformulated dropout in the encoder for learning

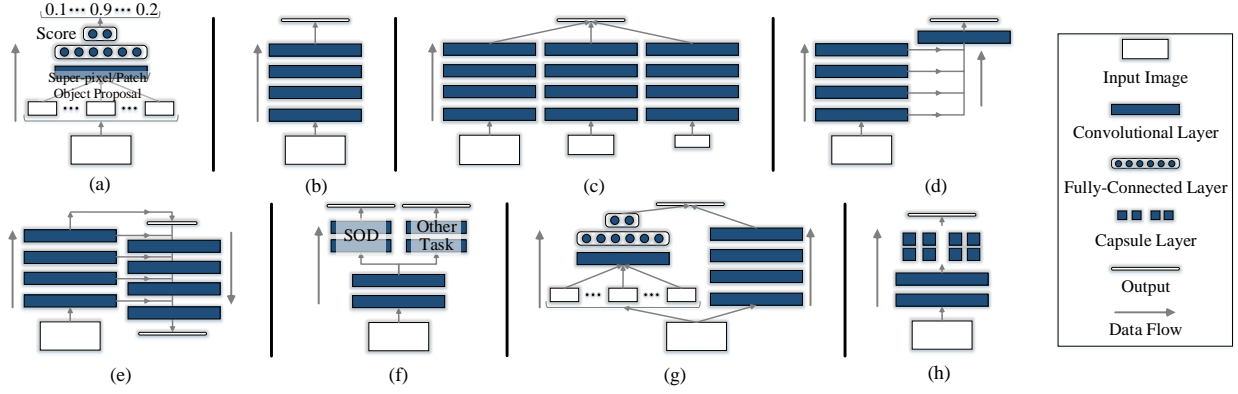


Fig. 2. Category of previous deep SOD models according to the adopted network architecture. (a) MLP-based methods. (b)-(f) FCN-based methods, mainly using (b) single-stream network, (c) multi-stream network, (d) side-out fusion network, (e) bottom-up/top-down network, and (f) branch network architectures. (g) Hybrid network-based methods. (h) Capsule-based methods. See §2.1 for more detailed descriptions.

uncertain features, and a hybrid up-sampling scheme in the decoder for avoiding checkerboard artifacts.

2) Multi-stream network, as depicted in Fig. 2(c), typically consists of multiple network streams to explicitly learning multi-scale saliency features from multi-resolution inputs. Multi-stream outputs are fused to form a final prediction.

- **MSRNet** [70] has three streams to process three scaled versions of input images. The three outputs are finally fused through a learnable attention module.

3) Side-fusion network fuses multi-layer responses of a backbone network together for SOD prediction, making use of the inherent multi-scale representations of the CNN hierarchy (Fig. 2(d)). Side-outputs are typically supervised by the ground-truth, leading to a *deep supervision* strategy [118].

- **DSS** [38] adds short connections from deeper side-outputs to shallower ones. Thus higher-level features help lower side-outputs better locate salient regions, and lower-level features can enrich deeper side-outputs with finer details.

4) Bottom-up/top-down network refines rough saliency maps in the feed-forward pass by gradually incorporating spatial-detail-rich features from lower layers, and produces the finest saliency maps at the top-most layer (Fig. 2(e)).

- **DGRL** [85] purifies low-level features before combining them with the high-level ones. The combined features are refined recurrently in a top-down pathway. The final output is enhanced by a boundary refinement submodule.

- **PiCANet** [39] hierarchically embeds global and local pixel-wise contextual attention modules into the top-down pathway of a U-Net [119] structure.

5) Branched network typically addresses multi-task learning for more robust saliency pattern modeling. It has a *single-input-multiple-output* structure, where bottom layers are shared to process a common input and top ones are specialized for different tasks (Fig. 2(f)).

- **C2S-Net** [99] is first constructed by adding a pre-trained contour detection model [120] to a main SOD branch. Then the two branches are alternately trained with the supervision for the two tasks, *i.e.*, SOD and contour detection.

2.1.3 Hybrid Network-based Methods

Some other models combine both MLP- and FCN-based subnets to produce edge-preserving results with multi-scale contexts (Fig. 2(g)). The combination of pixel-level and

region-level saliency cues is promising to yield improved performance, while bringing extra computational cost.

- **CRPSD** [105] combines pixel- and region-level saliency. The former is generated by fusing the last and penultimate side-output features of an FCN, while the latter is obtained by applying an existing SOD model [28] to image regions. Only the FCN and fusion layers are trainable.

2.1.4 Capsule-based Methods

Recently, Hinton *et al.* [59] propose a new network family, named *Capsule*. Capsules are made up of a group of neurons which accept and output vectors as opposed to CNNs' scalar values, allowing a comprehensively modeling of entity properties. Some researchers are thus inspired to explore Capsules in SOD [40], [41] (Fig. 2(h)).

- **TSPONet** [40] emphasizes part-object relations by a two-stream capsule network. The input features of capsules are extracted from a CNN, which are transformed into low-level capsules and assigned to high-level ones, and finally recognized to be salient or background.

2.2 Level of Supervision

Based on the form of supervision, deep SOD models can be classified into either *fully-supervised* or *un-/weakly-supervised*.

2.2.1 Fully-Supervised Methods

Most deep SOD models are trained with large-scale pixel-wise human annotations, suffering from time-consuming and expensive human labor. Moreover, models trained on fine-labeled datasets tend to overfit and generalize poorly to real-life images [67]. Thus, training SOD with weaker annotations becomes an increasingly popular research direction.

2.2.2 Un-/Weakly-Supervised Methods

To get rid of laborious manual labeling, diverse weak supervision forms are explored in un-/weakly supervised SOD methods, including *image-level category* labels [68], [97], *object contours* [99], *image captions* [81] and *pseudo groundtruth* masks generated by non-learning SOD methods [67], [83], [98].

1) Category-level supervision. It is evidenced that deep features trained with only image-level labels are also informative of object locations [121], [122], being promising to provide useful supervision signals for SOD training.

- **WSS** [97] first pre-trains a two-branch network to predict image labels at one branch using ImageNet [114], while

estimating saliency maps at the other. The estimated maps are refined by CRF and used to fine-tune the SOD branch.

2) Pseudo pixel-level supervision. Though informative, image-level labels are too weak. Some researchers instead use traditional non-learning SOD methods[67], [83], [98], or contour information[99], to generate noisy yet finer-grained cues for training.

- **SBF** [83] fuses weak saliency maps from a set of prior heuristic SOD models [34], [123], [124] at intra- and inter-image levels, to generate supervision signals.

2.3 Learning Paradigm

From the perspective of learning paradigms, SOD networks can be divided into methods of *single-task learning* (STL) and *multi-task learning* (MTL).

2.3.1 Single-Task Learning (STL) based Methods

In machine learning, the standard methodology is to learn one task at a time [125], *i.e.*, STL. Most deep SOD methods belong to this realm of learning paradigm, *i.e.*, utilize the supervision from a single knowledge domain (SOD or other related fields like image classification[68]) for training.

2.3.2 Multi-Task Learning (MTL) based Methods

Inspired by the human learning process where the knowledge learned from related tasks can assist the learning of a new task, MTL [125] aims to improve the performance of multiple related tasks by learning them simultaneously. Benefiting from extra knowledge from related tasks, models can gain improved generalizability. An extra advantage lies on the sharing of samples among tasks, which alleviates the lack of data for training heavy-parameterized models. These are the core motivations of MTL based SOD models and branched architectures (see §2.1.2) are usually adopted.

1) Salient object subitizing. The ability of humans to rapidly enumerate a small number of items is referred as subitizing [112], [126]. Some works learn salient object subitizing and detection simultaneously [36], [77], [79].

- **DSOS** [77] uses an auxiliary network to learn salient object subitizing. To encode numerical information into spatial representation, some parameters of the main SOD network are dynamically determined by the subitizing network.

2) Fixation prediction aims to predict human eye-fixation locations in visual scenes. Due to its close relation with SOD, learning shared knowledge from these two tasks is promising to improve the performances of both.

- **ASNet** [87] derives fixation information as a high-level understanding of the scene, from upper network layers. Then fine-grained object-level saliency is progressively optimized with the guidance of the fixation in a top-down manner.

3) Image classification. Image-level tags are valuable for SOD, as they provide the category information of dominant objects in the images which are much likely to be the salient regions[97]. Inspired by this observation, some SOD models learn image classification as an auxiliary task.

- **ASMO** [98] leverages class activation maps from a neural classifier and saliency maps from prior non-learning SOD methods to train the SOD network, in an iterative manner.

4) Semantic segmentation is for per-pixel semantic prediction. Though SOD is class-agnostic, high-level semantics

play a crucial role in saliency modeling. Thus the task of semantic segmentation is also integrated into SOD learning.

- **SSNet** [103] learns semantic segmentation and SOD jointly, which is achieved by a saliency aggregation module that predicts the saliency of each category and aggregates the segmentation masks of all categories into a saliency map.

5) Contour/edge detection refers to the task of detecting obvious object boundaries in images, which are informative of salient objects. Thus it is also explored in SOD modeling.

- **PAGE-Net** [92] learns an edge detection module and embeds edge information into the main SOD stream in a top-down manner, leading to better edge-preserving results.

6) Image Captioning can provide extra knowledge about the main content of visual scenes, enabling SOD models to better capture high-level semantics.

- **CapSal** [100] leverages captioning to promote SOD. It incorporates semantic context from a captioning network with local-global visual cues for final saliency prediction.

2.4 Object-/Instance-Level SOD

According to whether being able to identify different salient object instances, current deep SOD models can be categorized into *object-level* ones and *instance-level* ones.

2.4.1 Object-Level Methods

Most deep SOD models are object-level methods, *i.e.*, designed to detect pixels that belong to salient objects without being aware of individual object instances.

2.4.2 Instance-Level Methods

Instance-level SOD methods further identify individual object instances in the detected salient regions, which is crucial for practical applications that need finer distinctions, such as semantic segmentation[131] and multi-human parsing[132].

- **MSRNet** [70] first learns object-level SOD and salient contour detection jointly. Then a set of object proposals are derived from the detected contours and refined by the estimated saliency scores, for final instance-level prediction.

3 SOD DATASETS

With the rapid development of SOD, numerous datasets have been introduced. Table 4 summarizes 19 SOD datasets, which are highly representative and widely used for training or benchmarking, or collected with specific properties.

3.1 Quick Overview

In an attempt to facilitate understanding of SOD datasets, we present here some take-away points of this section.

- Compared with early datasets [29], [30], [127], recent ones [26], [56], [97], [107] are typically more advanced with less center bias, improved complexity, increased scale, thus better suiting for training/testing and having longer life-span.
- Some other recent datasets [70], [73], [100], [112], [129], [130] are enriched with more diverse annotations (*e.g.*, subitizing, captioning), representing new trends in the field.

More in-depth discussions regarding generalizability and hardness of several famous datasets will be presented at §5.6.

TABLE 4

Statistics of popular SOD datasets, including the number of images, the number of salient objects per image, the area ratio of the salient objects per image, annotation type, image resolution, and the existence of fixation data. See §3 for more detailed descriptions.

	Dataset	Year	Publ.	#Img.	#Obj.	Obj. Area(%)	SOD Annotation	Resolution	Fix.
Early	MSRA-A [29]	2007	CVPR	1,000/20,840	1-2	-	bounding-box object-level	-	
	MSRA-B [29]	2007	CVPR	5,000	1-2	20.82 \pm 10.29	bounding-box object-level, pixel-wise object-level	max(w, h) = 400, min(w, h) = 126	
	SED1 [127]	2007	CVPR	100	1	26.70 \pm 14.26	pixel-wise object-level	max(w, h) = 465, min(w, h) = 125	
	SED2 [127]	2007	CVPR	100	2	21.42 \pm 18.41	pixel-wise object-level	max(w, h) = 300, min(w, h) = 144	
	ASD [30]	2009	CVPR	1,000	1-2	19.89 \pm 9.53	pixel-wise object-level	max(w, h) = 400, min(w, h) = 142	
Modern&Popular	SOD [128]	2010	CVPR-W	300	1-4+	27.99 \pm 19.36	pixel-wise object-level	max(w, h) = 481, min(w, h) = 321	
	MSRA10K [107]	2015	TPAMI	10,000	1-2	22.21 \pm 10.09	pixel-wise object-level	max(w, h) = 400, min(w, h) = 144	
	ECSSD [55]	2015	TPAMI	1,000	1-4+	23.51 \pm 14.02	pixel-wise object-level	max(w, h) = 400, min(w, h) = 139	
	DUT-OMRON [56]	2013	CVPR	5,168	1-4+	14.85 \pm 12.15	pixel-wise object-level	max(w, h) = 401, min(w, h) = 139	✓
	PASCAL-S [108]	2014	CVPR	850	1-4+	24.23 \pm 16.70	pixel-wise object-level	max(w, h) = 500, min(w, h) = 139	✓
	HKU-IS [26]	2015	CVPR	4,447	1-4+	19.13 \pm 10.90	pixel-wise object-level	max(w, h) = 500, min(w, h) = 100	
	DUTS [97]	2017	CVPR	15,572	1-4+	23.17 \pm 15.52	pixel-wise object-level	max(w, h) = 500, min(w, h) = 100	
	SOS [112]	2015	CVPR	6,900	0-4+	41.22 \pm 25.35	object number, bounding-box (<i>train</i> set)	max(w, h) = 6132, min(w, h) = 80	
Special	MSO [112]	2015	CVPR	1,224	0-4+	39.51 \pm 24.85	object number, bounding-box instance-level	max(w, h) = 3888, min(w, h) = 120	
	ILSO [70]	2017	CVPR	1,000	1-4+	24.89 \pm 12.59	pixel-wise instance-level	max(w, h) = 400, min(w, h) = 142	
	XPIE [129]	2017	CVPR	10,000	1-4+	19.42 \pm 14.39	pixel-wise object-level, geographic information	max(w, h) = 500, min(w, h) = 130	✓
	SOC [130]	2018	ECCV	6,000	0-4+	21.36 \pm 16.88	pixel-wise instance-level, object category, attribute	max(w, h) = 849, min(w, h) = 161	
	COCO-CapSal [100]	2019	CVPR	6,724	1-4+	23.74 \pm 17.00	pixel-wise object-level, image caption	max(w, h) = 640, min(w, h) = 480	
	HRSOD [73]	2019	ICCV	2,010	1-4+	21.13 \pm 15.14	pixel-wise object-level	max(w, h) = 10240, min(w, h) = 600	

3.2 Early SOD Datasets

Early SOD datasets typically contain simple scenes where 1~2 salient objects stand out from clear background.

- **MSRA-A [29]** contains 20,840 images. Each image has only one noticeable and eye-attracting object, annotated by a bounding-box. As a subset of MSRA-A, MSRA-B has 5,000 images and less ambiguity w.r.t. the salient object.
- **SED [127]**¹ comprises of a single-object subset and a two-object subset; each has 100 images with mask annotations.
- **ASD [30]**², also a subset of MSRA-A, has 1,000 images with pixel-wise ground-truths.

3.3 Modern Popular SOD Datasets

Recently emerged datasets tend to include more challenging and general scenes with relatively complex backgrounds and multiple salient objects. All have pixel-wise annotations.

- **SOD [128]**³ consists of 300 images, constructed from [133]. Many images have more than one salient object which is similar to the background or touches image boundaries.
- **MSRA10K [107]**⁴, also known as THUS10K, contains 10,000 images selected from MSRA-A and covers all the images in ASD. Due to its large scale, MSRA10K is widely used to train deep SOD models (see Table 3).
- **ECSSD [55]**⁵ is composed by 1,000 images with semantically meaningful but structurally complex natural contents.
- **DUT-OMRON [56]**⁶ has 5,168 images of complex backgrounds and diverse content, with pixel-wise annotations.
- **PASCAL-S [108]**⁷ has 850 challenging images selected from PASCAL VOC2010 *val* set [113]. With eye-fixation records, non-binary salient-object mask annotations are provided, where the saliency value of a pixel is calculated as the ratio of subjects that select the segment containing this pixel as salient.
- **HKU-IS [26]**⁸ contains 4,447 complex scenes that typically contain multiple disconnected objects with diverse spatial distribution and similar fore-/back-ground appearance.

- **DUTS [97]**⁹ is a large dataset, where 10,553 training images are selected from ImageNet *train/val* set [114], and 5,019 test images are from ImageNet *test* set and SUN [134]. Since 2017, SOD models are typically trained on DUTS (Table 3).

3.4 Other Special SOD Datasets

Beyond above “standard” SOD datasets, some special ones are proposed recently, leading to new research directions.

- **SOS [112]**¹⁰ is created for SOD subitizing [126]. It contains 6,900 images (*training* set: 5,520, *test* set: 1,380). Each image is labeled as containing 0, 1, 2, 3 or 4+ salient objects.
- **MSO [112]**¹¹ is a subset of SOS-*test* [112], covering 1,224 images. It has a more balanced distribution of the number of salient objects. Each object has a bounding box annotation.
- **ILSO [70]**¹² contains 1,000 images with pixel-wise instance-level annotations and coarse contour labeling.
- **XPIE [129]**¹³ has 10,000 images with pixel-wise labels. It has three subsets: *Set-P* has 625 images of places-of-interest with geographic information; *Set-I* 8,799 images with object tags; and *Set-E* 576 images with eye-fixation records.
- **SOC [130]**¹⁴ consists of 6,000 images with 80 common categories. Half of the images contain salient objects and the others have none. Each salient-object-contained image is annotated with instance-level ground-truth mask, object category, and challenging factors. The non-salient object subset has 783 texture images and 2,217 real-scene images.
- **COCO-CapSal [100]**¹⁵ is built from COCO [115] and SALICON [111]. Salient objects are first roughly localized using the mouse-click data in SALICON, then precisely annotated according to the instance masks in COCO. The dataset has 5,265 and 1,459 images for training and testing, respectively.
- **HRSOD [73]**¹⁶ is the first *high-resolution* dataset for SOD. It contains 1,610 training images and 400 testing images collected from website. Pixel-wise ground-truths are provided.

1. http://www.wisdom.weizmann.ac.il/~vision/Seg_Evaluation_DB

2. https://ivrlwww.epfl.ch/supplementary_material/RK_CVPR09/

3. <http://elderlab.yorku.ca/SOD/>

4. <https://mmcheng.net/zh/msra10k/>

5. <http://www.cse.cuhk.edu.hk/leojia/projects/hsaliency>

6. <http://saliencydetection.net/dut-omron/>

7. <http://cbi.gatech.edu/salobj/>

8. https://i.cs.hku.hk/~gbli/deep_saliency.html

9. <http://saliencydetection.net/duts/>

10. <http://cs-people.bu.edu/jmzhang/sos.html>

11. <http://cs-people.bu.edu/jmzhang/sos.html>

12. <http://www.sysu-hcp.net/instance-level-salient-object-segmentation/>

13. <http://cvteam.net/projects/CVPR17-ELE/ELE.html>

14. <http://mmcheng.net/SOCBenchmark/>

15. <https://github.com/yi94code/HRSOD>

16. <https://github.com/zhangludl/code-and-dataset-for-CapSal>

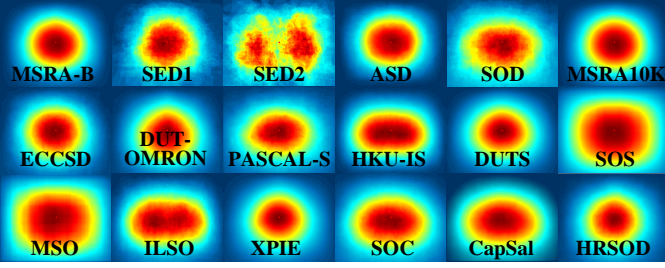


Fig. 3. Annotation distributions of SOD datasets (see §3 for details).

3.5 Discussion

As shown in Table 4, *early SOD datasets* [29], [30], [127] collect simple images with 1~2 salient objects per image, and only provide rough bounding box annotations that were thought to be insufficient for reliable evaluations [30], [135]. The performances on these datasets become saturated. *Modern datasets* [26], [55], [56], [97], [107] are typically large-scale and offer precise pixel-wise ground-truths. The scenes are more complex and general, and usually contain multiple salient objects. Some *special datasets* contain challenging scenes with background only [112], [130], provide more fine-grained, instance-level SOD groundtruths [70], [130] and other annotations like image captions [100], inspiring new research directions and applications. Fig. 3 depicts annotation distributions of 18 SOD datasets. Here are some essential conclusions: 1) some datasets [29], [30], [97], [107] have significant center bias; 2) [26], [70], [100] have more balanced location distribution of salient object; and 3) the center bias in [112] looks more less as only bounding-box annotations are provided. We in-depth analyze the generalizability and difficulty of several famous SOD datasets in §5.6.

4 EVALUATION METRICS

This section reviews popular object-level SOD evaluation metrics, *i.e.*, Precision-Recall (PR), F-measure [30], Mean Absolute Error (MAE) [32], weighted F_β measure (Fbw) [136], Structural measure (S-measure) [137], and Enhanced-alignment measure (E-measure) [138].

4.1 Quick Overview

To better understand the characteristics of metrics, a quick overview of main conclusions of this section is shown here.

- PR, F-measure, MAE, and Fbw address *pixel-wise* errors, while S-measure and E-measure consider *structure* cues.
- Among pixel-level metrics, PR, F-measure, and Fbw fail to consider true negative pixels, while MAE can remedy this.
- Among structured metrics, S-measure is more favored than E-measure, as SOD addresses continuous saliency estimates.
- Considering popularity, advantages and completeness, F-measure, S-measure and MAE are the most recommended and used for our performance benchmarking in §5.2.

4.2 Metric Details

- **PR** is calculated based on binarized salient object mask and ground-truth:

$$\text{Precision} = \frac{TP}{TP + FP}, \quad \text{Recall} = \frac{TP}{TP + FN}, \quad (1)$$

where TP, TN, FP, FN denote true-positive, true-negative,

false-positive, and false-negative, respectively. A set of thresholds ($[0 - 255]$) is applied to binarize the prediction. Each threshold produces a pair of Precision/Recall value to form a PR curve for describing model performance.

- **F-measure** [30] comprehensively considers both Precision and Recall by computing the weighted harmonic mean:

$$F_\beta = \frac{(1 + \beta^2)\text{Precision} \times \text{Recall}}{\beta^2\text{Precision} + \text{Recall}}. \quad (2)$$

β^2 is empirically set to 0.3 [30] to emphasize more on Precision. Instead of plotting the whole F-measure curve, some methods only report *maximal* F_β , or binarize the predicted saliency map by an adaptive threshold, *i.e.*, twice the mean value of the saliency prediction, and report *mean* F .

- **MAE** [32] measures the average pixel-wise absolute error between normalized saliency prediction map $S \in [0, 1]^{W \times H}$ and binary groundtruth mask $G \in \{0, 1\}^{W \times H}$:

$$\text{MAE} = \frac{1}{W \times H} \sum_{i=1}^W \sum_{j=1}^H |G(i, j) - S(i, j)|. \quad (3)$$

- **Fbw** [136] intuitively generalizes F-measure by alternating the way to calculate Precision and Recall. It extends the four basic quantities TP, TN, FP and FN to real values, and assigns different weights (ω) to different errors at different locations considering the neighborhood information:

$$F_\beta^\omega = \frac{(1 + \beta^2)\text{Precision}^\omega \times \text{Recall}^\omega}{\beta^2\text{Precision}^\omega + \text{Recall}^\omega}. \quad (4)$$

- **S-measure** [137] evaluates structural similarity between the real-valued saliency map and the binary ground-truth. It considers object-aware (S_o) and region-aware (S_r) structure similarities:

$$S = \alpha \times S_o + (1 - \alpha) \times S_r, \quad (5)$$

where α is empirically set to 0.5.

- **E-measure** [138] considers global means of the image and local pixel matching simultaneously:

$$Q_S = \frac{1}{W \times H} \sum_{i=1}^W \sum_{j=1}^H \phi_S(i, j), \quad (6)$$

where ϕ_S is the enhanced alignment matrix, reflecting the correlation between S and G after subtracting their global means, respectively.

4.3 Discussion

These measures are typically based on *pixel-wise* errors while ignoring *structural* similarities, only except for S-measure and E-measure. F-measure and E-measure are designed for assessing *binarized* saliency prediction maps, while PR, MAE, Fbw, and S-measure are for *non-binary* map evaluation.

Among pixel-level metrics, PR curve is classic, but precision and recall cannot fully assess the quality of saliency predictions, since high-precision predictions may only highlight a part of salient objects, and high-recall ones can be meaningless if all the pixels are predicted as salient. In general, a high-recall response may come at the expense of reduced precision, and vice versa. F-measure and Fbw are thus used to consider precision and recall simultaneously. However, overlap-based metrics (*i.e.*, PR, F-measure, and Fbw) do not consider the true negative saliency assignments, *i.e.*, the pixels correctly marked as non-salient. Thus these metrics favor methods that successfully assign

TABLE 5

Benchmarking results of 44 state-of-the-art deep SOD models and 3 top-performing classic SOD methods on 6 famous datasets (§5.2). Here max F, S, and M indicate *maximal* F_β , S-measure, and MAE, respectively. The three best scores are marked in **red**, **blue**, and **green**, respectively.

Dataset		ECSSD [55]			DUT-OMRON [56]			PASCAL-S [108]			HKU-IS [26]			DUTS-test [97]			SOD [128]		
Metric		max F↑	S↑	M↓	max F↑	S↑	M↓	max F↑	S↑	M↓	max F↑	S↑	M↓	max F↑	S↑	M↓	max F↑	S↑	M↓
2013-14	*HS [34]	.673	.685	.228	.561	.633	.227	.569	.624	.262	.652	.674	.215	.504	.601	.243	.756	.711	.222
	*DRFI [53]	.751	.732	.170	.623	.696	.150	.639	.658	.207	.745	.740	.145	.600	.676	.155	.658	.619	.228
	*wCtr [35]	.684	.714	.165	.541	.653	.171	.599	.656	.196	.695	.729	.138	.522	.639	.176	.615	.638	.213
2015	MCDL [28]	.816	.803	.101	.670	.752	.089	.706	.721	.143	.787	.786	.092	.634	.713	.105	.689	.651	.182
	LEGS [27]	.805	.786	.118	.631	.714	.133	‡	‡	‡	.736	.742	.119	.612	.696	.137	.685	.658	.197
	MDF [26]	.797	.776	.105	.643	.721	.092	.704	.696	.142	.839	.810	.129	.657	.728	.114	.736	.674	.160
2016	ELD [60]	.849	.841	.078	.677	.751	.091	.782	.799	.111	.868	.868	.063	.697	.754	.092	.717	.705	.155
	DHSNet [37]	.893	.884	.060	‡	‡	‡	.799	.810	.092	.875	.870	.053	.776	.818	.067	.790	.749	.129
	DCL [104]	.882	.868	.075	.699	.771	.086	.787	.796	.113	.885	.877	.055	.742	.796	.149	.786	.747	.195
	◊MAP [36]	.556	.611	.213	.448	.598	.159	.521	.593	.207	.552	.624	.182	.453	.583	.181	.509	.557	.236
	CRPSD [105]	.915	.895	.048	-	-	-	.864	.852	.064	.906	.885	.043	-	-	-	-	-	-
	RFCN [63]	.875	.852	.107	.707	.764	.111	.800	.798	.132	.881	.859	.089	.755	.859	.090	.769	.794	.170
2017	MSRNet [70]	.900	.895	.054	.746	.808	.073	.828	.838	.081	‡	‡	‡	.804	.839	.061	.802	.779	.113
	DSS [38]	.906	.882	.052	.737	.790	.063	.805	.798	.093	‡	‡	‡	.796	.824	.057	.805	.751	.122
	†WSS [97]	.879	.811	.104	.725	.730	.110	.804	.744	.139	.878	.822	.079	.878	.822	.079	.807	.675	.170
	DLS [65]	.826	.806	.086	.644	.725	.090	.712	.723	.130	.807	.799	.069	-	-	-	-	-	-
	NLDF [75]	.889	.875	.063	.699	.770	.080	.795	.805	.098	.888	.879	.048	.777	.816	.065	.808	.889	.125
	Amulet [76]	.905	.894	.059	.715	.780	.098	.805	.818	.100	.887	.886	.051	.750	.804	.085	.773	.757	.142
	FSN [72]	.897	.884	.053	.736	.802	.066	.800	.804	.093	.884	.877	.044	.761	.808	.066	.781	.755	.127
	SBF [83]	.833	.832	.091	.649	.748	.110	.726	.758	.133	.821	.829	.078	.657	.743	.109	.740	.708	.159
	SRM [71]	.905	.895	.054	.725	.798	.069	.817	.834	.084	.893	.887	.046	.798	.836	.059	.792	.741	.128
2018	UCF [66]	.890	.883	.069	.698	.760	.120	.787	.805	.115	.874	.875	.062	.742	.782	.112	.763	.753	.165
	RADF [78]	.911	.894	.049	.761	.817	.055	.800	.802	.097	.902	.888	.039	.792	.826	.061	.804	.757	.126
	BDMP [84]	.917	.911	.045	.734	.809	.064	.830	.845	.074	.910	.907	.039	.827	.862	.049	.806	.786	.108
	DGRL [85]	.916	.906	.043	.741	.810	.063	.830	.839	.074	.902	.897	.037	.805	.842	.050	.802	.771	.105
	PAGR [86]	.904	.889	.061	.707	.775	.071	.814	.822	.089	.897	.887	.048	.817	.838	.056	.761	.716	.147
	RSDNet [79]	.880	.788	.173	.715	.644	.178	‡	‡	‡	.871	.787	.156	.798	.720	.161	.790	.668	.226
	ASNet [87]	.925	.915	.047	‡	‡	‡	.848	.861	.070	.912	.906	.041	.806	.843	.061	.801	.762	.121
	PiCANet [39]	.929	.916	.035	.767	.825	.054	.838	.846	.064	.913	.905	.031	.840	.863	.040	.814	.776	.096
	†C2S-Net [99]	.902	.896	.053	.722	.799	.072	.827	.839	.081	.887	.889	.046	.784	.831	.062	.786	.760	.124
2019	RAS [88]	.908	.893	.056	.753	.814	.062	.800	.799	.101	.901	.887	.045	.807	.839	.059	.810	.764	.124
	AFNet [89]	.924	.913	.042	.759	.826	.057	.844	.849	.070	.910	.905	.036	.838	.867	.046	.809	.774	.111
	BASNet [90]	.931	.916	.037	.779	.836	.057	.835	.838	.076	.919	.909	.032	.838	.866	.048	.805	.769	.114
	CapSal [100]	.813	.826	.077	.535	.674	.101	.827	.837	.073	.842	.851	.057	.772	.818	.061	.669	.694	.148
	CPD [80]	.926	.918	.037	.753	.825	.056	.833	.848	.071	.911	.905	.034	.840	.869	.043	.814	.767	.112
	MLSLNet [91]	.917	.911	.045	.734	.809	.064	.835	.844	.074	.910	.907	.039	.828	.862	.049	.806	.786	.108
	†MWS [81]	.859	.827	.099	.676	.756	.108	.753	.768	.134	.835	.818	.086	.720	.759	.092	.772	.700	.170
	PAGE-Net [92]	.926	.910	.037	.760	.819	.059	.829	.835	.073	.910	.901	.031	.816	.848	.048	.795	.763	.108
	PS [94]	.930	.918	.041	.789	.837	.061	.837	.850	.071	.913	.907	.038	.835	.865	.048	.824	.800	.103
2020	PoolNet [93]	.937	.926	.035	.762	.831	.054	.858	.865	.065	.923	.919	.030	.865	.886	.037	.831	.788	.106
	BANet-R [101]	.939	.924	.035	.782	.832	.059	.847	.852	.070	.923	.913	.032	.858	.879	.040	.842	.791	.106
	EGNet-R [82]	.936	.925	.037	.777	.841	.053	.841	.852	.074	.924	.918	.031	.866	.887	.039	.854	.802	.099
	HRSOD-DH [73]	.911	.888	.052	.692	.762	.065	.810	.817	.079	.890	.877	.042	.800	.824	.050	.735	.705	.139
	JDFPR [95]	.915	.907	.049	.755	.821	.057	.827	.841	.082	.905	.903	.039	.792	.836	.059	.792	.763	.123
	SCRN [102]	.937	.927	.037	.772	.836	.056	.856	.869	.063	.921	.916	.034	.864	.885	.040	.826	.787	.107
	SSNet [103]	.889	.867	.046	.708	.773	.056	.793	.807	.072	.876	.854	.041	.769	.784	.049	.713	.700	.118
	TSPOANet [40]	.919	.907	.047	.749	.818	.061	.830	.842	.078	.909	.902	.039	.828	.860	.049	.810	.772	.118

* Non-deep learning model. † Weakly-supervised model. ◊ Bounding-box output. ‡ Training on subset. - Results not available.

high saliency to salient pixels but fail to detect non-salient regions [49]. MAE can remedy this, but it performs poorly when salient objects are small. For the structure-/image-level metrics, S-measure is more popular than E-measure, since SOD focuses on continuous predictions.

Considering the popularity and characteristics of existing metrics and completeness of evaluation, F-measure (*maximal* F_β), S-measure and MAE are our top recommendations.

5 BENCHMARKING AND EMPIRICAL ANALYSIS

This section provides empirical analyses to shed light on some key challenges in the field. Specifically, with our large-scale benchmarking results (§5.2), we first perform attribute-based study to better understand the benefits and limitations of current arts (§5.3). Then, we study the robustness of SOD models against input perturbations, *i.e.*, random exerted noises (§5.4) and manually designed adversarial samples (§5.5). Finally, we quantitatively assess the generalizability and hardness of current main-stream datasets (§5.6).

5.1 Quick Overview

For ease of understanding, we collect here essential observations and conclusions from subsequent experiments.

- *Overall benchmarks* (§5.2). As shown in Table 5, deep SOD models significantly outperforms heuristic ones and the performances on some datasets [26], [55] have been saturated. [82], [93], [101], [102] are current state-of-the-arts.

- *Attribute-based analysis* (§5.3). Attribute-based results in Table 7 reveal that deep methods show significant advantages in semantic-rich objects, such as animal. Both deep and non-deep methods face difficulties with small salient objects. For application scenarios, indoor scenes pose great challenges, demonstrating the potential directions of future efforts.

- *Robustness against random perturbations* (§5.4). As shown in Table 9, surprisingly, deep methods are more sensitive than heuristic ones for random input perturbations. Both types of methods show more robust against *Rotation*, while being fragile towards *Gaussian blur* and *Gaussian noise*.

- *Adversarial attack* (§5.5). Table 10 suggests that adversarial



Fig. 4. Sample images from the hybrid benchmark consisting of images randomly selected from 6 SOD datasets. Saliency regions are uniformly highlighted. Corresponding attributes are listed. See §5.3 for more detailed descriptions.

TABLE 7

Attribute-based study w.r.t. salient object categories, challenges and scene categories. (·) indicates the percentage of the images with a specific attribute. *ND-avg* indicates the average score of three heuristic models: HS [34], DRFI [53] and wCtr [35]. *D-avg* indicates the average score of three deep learning models: DGRL [85], PAGR [86] and PiCANet [39]. Best in **red**, and worst with **underline**. See §5.3 for more details.

Metric	Method	Salient object categories				Challenges									Scene categories		
		<i>Human</i> (26.61)	<i>Animal</i> (38.44)	<i>Artifact</i> (45.67)	<i>NatObj</i> (10.56)	<i>MO</i> (11.39)	<i>HO</i> (66.39)	<i>OV</i> (28.72)	<i>OC</i> (46.50)	<i>CS</i> (40.44)	<i>BC</i> (47.22)	<i>CT</i> (74.11)	<i>SO</i> (21.61)	<i>LO</i> (12.61)	<i>Indoor</i> (20.28)	<i>Urban</i> (22.22)	<i>Natural</i> (57.50)
max $F\uparrow$	*HS [34]	.587	.650	.636	.704	.663	.637	.631	.645	.558	.647	.629	.493	.737	.594	.627	.650
	*DRFI [53]	.635	.692	.673	.713	.674	.688	.658	.675	.599	.662	.677	.566	.747	.609	.661	.697
	*wCtr [35]	.557	.621	.624	.682	.639	.625	.605	.620	.522	.612	.606	.469	.689	.578	.613	.618
	DGRL [85]	.820	.881	.830	.728	.783	.846	.829	.830	.781	.842	.834	.724	.873	.800	.848	.840
	PAGR [86]	.834	.890	.787	.725	.743	.819	.778	.809	.770	.797	.822	.760	.802	.788	.796	.828
	PiCANet [39]	.840	.897	.846	.669	.791	.861	.843	.845	.797	.848	.850	.763	.889	.806	.862	.859
	*ND-avg	.593	.654	.644	.700	.659	.650	.631	.647	.560	.640	.637	.509	.724	.594	.634	.655
	D-avg	.831	.889	.821	.708	.772	.842	.817	.828	.783	.829	.836	.749	.855	.798	.836	.842

* Non-deep learning model.

attacks cause drastic performance degrades for deep SOD models, even worse than that of random perturbations. But the attack rarely transfers among different SOD networks.

- *Generalizability and hardness of datasets* (§5.6). Table 11 evidences that DUTS-train [97] is a good choice for training deep SOD models as it has the best generalizability, SOC [130], DUT-OMRON [56], and DUTS-test [97] are more suitable for evaluation due to their hardness.

5.2 Performance Benchmarking

Table 5 shows performances of 44 state-of-the-art deep SOD models and 3 top-performing classic methods (suggested by [43]) on 6 most popular modern datasets. The performance is measured by three metrics, *i.e.*, maximal $F\beta$, S-measure and MAE, recommended in §4.3. All the benchmarked models are representative, and have publicly available implementations or saliency prediction results.

Not surprisingly, data-driven models greatly outperform conventional heuristic ones, due to their strong learning ability for visually salient pattern modeling. In addition, the performance gradually increased over time since 2015, well demonstrating the advance of deep learning techniques. However, after 2018, the increasing velocity of performance reduced, calling for more effective model designs and new machine learning technologies.

We can also find the performances tend to be saturated on older-fashioned SOD datasets such as ECSSD [55] and HKU-IS [26]. Hence, among the 44 famous deep SOD models, we would like to nominate PoolNet [93], BANet [101], EGNet [82], and SCRNet [102] as the 4 state-of-the-art methods, which show promising performance over diverse datasets consistently.

5.3 Attribute-Based Study

Although the community witnessed the great advance made by deep SOD models, it is still unclear on what specific aspects these models perform well or not. As there are numerous factors affect the performance of a SOD algorithm, such as object/scene category, occlusion, it is crucial to

TABLE 6

Descriptions of attributes regarding the challenging factors that often bring difficulties to SOD. See §5.3 for more details.

Attr	Description
<i>MO</i> Multiple Objects .	There exist more than two salient objects.
<i>HO</i> Heterogeneous Object .	Salient object regions have distinct colors or illuminations.
<i>OV</i> Out-of-view .	Salient objects are partially clipped by image boundaries.
<i>OC</i> Occlusion .	Salient objects are occluded by other objects.
<i>CS</i> Complex Scene .	Background regions contain confusing objects or rich details.
<i>BC</i> Background Clutter .	Foreground and background regions around the salient object boundaries have similar colors (χ^2 between RGB histograms less than 0.9).
<i>CT</i> Complex Topology .	Salient objects have complex shapes, <i>e.g.</i> , thin parts or holes.
<i>SO</i> Small Object .	Ratio between salient object area and image is less than 0.1.
<i>LO</i> Large Object .	Ratio between salient object area and image is larger than 0.5.

evaluate the performance under certain scenarios. This can help in-depth demonstrate strength and weakness of deep SOD models, identify pending challenges, and point out future research directions towards more robust algorithms.

5.3.1 Hybrid Benchmark Dataset with Attribute Annotations

To enable a deeper analysis and understanding of the performance of an algorithm, it is essential to identify the key factors and circumstances which might have influenced it [139]. To this end, we construct a *hybrid benchmark* with rich attribute annotations. It consists of 1,800 images randomly selected from 6 SOD datasets (300 each), namely SOD [128], ECSSD [55], DUT-OMRON [56], PASCAL-S [108], HKU-IS [26] and DUTS test set [97]. Inspired by [108], [139], we annotate each image with an extensive set of attributes covering typical object types, challenging factors and diverse scene categories. Specifically, the annotated **salient objects** are categorized into *Human*, *Animal*, *Artifact* and *NatObj* (Natural Objects), where *NatObj* includes natural objects

TABLE 8

Attribute statistics of top and bottom 100 images based on F-measure. (·) indicates the percentage of the images with a specific attribute. *ND-avg* indicates the average results of three heuristic models: HS [34], DRFI [53] and wCtr [35]. *D-avg* indicates the average results of three deep models: DGRL [85], PAGR [86] and PiCANet [39]. Two largest changes in **red** if positive, and **blue** if negative. See §5.3 for more details.

Method	Cases	Salient object categories				Challenges										Scene categories		
		Human (26.61)	Animal (38.44)	Artifact (45.67)	NatObj (10.56)	MO (11.39)	HO (66.39)	OV (28.72)	OC (46.50)	CS (40.44)	BC (47.22)	CT (74.11)	SO (21.61)	LO (12.61)	Indoor (20.28)	Urban (22.22)	Natural (57.50)	
ND-avg	Best (%)	13.00	25.00	46.00	27.00	5.00	61.00	12.00	26.00	10.00	20.00	63.00	5.00	18.00	17.00	6.00	12.00	
	change	-13.61	-13.44	+0.33	+14.44	-6.39	-5.39	-16.72	-20.50	-30.44	-27.22	-11.11	-16.61	+5.39	-3.28	-16.22	-45.50	
D-avg	Worst (%)	36.00	30.00	41.00	5.00	6.00	54.00	15.00	34.00	70.00	31.00	71.00	76.00	0.00	22.00	37.00	37.00	
	change	+9.39	-8.44	-4.67	-5.56	-5.39	-12.39	-13.72	-12.50	+29.56	-16.22	-3.11	+54.39	-12.61	+1.72	+14.78	-20.50	
D-avg	Best (%)	24.00	30.00	49.00	17.00	3.00	69.00	33.00	28.00	26.00	35.00	49.00	2.00	18.00	24.00	23.00	53.00	
	change	-2.61	-8.44	+3.33	+6.44	-8.39	+2.61	+4.28	-18.50	-14.44	-12.22	-25.11	-19.61	+5.39	+3.72	+0.78	-4.50	
D-avg	Worst (%)	30.00	10.00	49.00	33.00	20.00	52.00	28.00	46.00	70.00	42.00	59.00	50.00	3.00	32.00	23.00	45.00	
	change	+3.39	-28.44	+3.33	+22.44	+8.61	-14.39	-0.72	-0.50	+29.56	-5.22	-15.11	+28.39	-9.61	+11.72	+0.78	-12.50	

such as fruit, plant, mountains, icebergs, lakes, *etc.* The **challenging factors** describe specific situations that often bring difficulties to SOD, such as occlusion, background cluster, and complex shape (see Table 6). The **scene** of images includes *Indoor*, *Urban* and *Natural*, where the last two indicate different outdoor environments. Please note that the attributes are not mutually exclusive. Some sample images with attribute annotations are shown in Fig. 4. Please note that this benchmark will also be used in §5.4 and §5.5.

For baselines, we choose the three top-performing heuristic models again, *i.e.*, HS [34], DRFI [53] and wCtr [35], and three recent famous deep methods, *i.e.*, DGRL [85], PAGR [86] and PiCANet [39] to perform attribute-based analysis. All the three deep models are trained on DUTS-*train* [97] and with publicly released implementations.

5.3.2 Analysis

In Table 7, we report the performance on subsets of our hybrid dataset characterized by a particular attribute. To enable a comprehensive insight, in Table 8, we select images with the best-100 and worst-100 model predictions and compare the portion distributions of attributes w.r.t. the ones over the whole dataset. Below are some salient and essential observations drawn from these experiments.

- **‘Easy’ and ‘Hard’ object categories.** Deep and non-deep SOD models view object categories differently (Table 7). For the deep methods (*D-avg*), *NatObj* is clearly the most challenging one which is probably due to small amount of training samples and complex topologies. *Animal* appears to be the easiest, which can be attributed to the significant semantics. By contrast, traditional methods (*ND-avg*) are short at *Human*, revealing their limitations in high-level semantics capturing. We are surprised to find, the deep models significantly outperform the non-deep ones over almost all the object categories, only except *NatObj*. This demonstrates the value of heuristic assumptions in certain scenes and the potential of embedding human prior knowledge into current deep learning schemes.
- **Most and least challenging factors.** Table 7 shows that, interestingly, both deep and non-deep methods handle *LO* well. In addition, both two types of methods face difficulties with *SO*, demonstrating a promising direction of future efforts. We can also observe that *CS* and *MO* are challenging for deep models, showing that current solutions are still short at reasoning the relative importance among objects.
- **Most and least difficult scenes.** Deep and heuristic methods perform similarly when facing different scenes (see

TABLE 9

Input perturbation study on the **hybrid benchmark**. *ND-avg* indicates the average score of three heuristic models: HS [34], DRFI [53] and wCtr [35]. *D-avg* indicates the average score of three deep learning models: SRM [71], DGRL [85] and PiCANet [39]. Best in **red** and worst with **underline**. See §5.4 for more details.

Metric	Method	Original	Gaus. blur (σ =)		Gaus. noise (var =)		Rotation 15° -15°		Gray
			2	4	0.01	0.08	15°	-15°	
max F \uparrow	*HS [34]	.600	-.012	-.096	-.022	-.057	+0.015	+0.009	-.104
	*DRFI [53]	.670	-.040	-.103	-.035	-.120	-.009	-.009	-.086
	*wCtr [35]	.611	+0.006	-.000	-.024	-.136	-.004	-.003	-.070
	SRM [71]	.817	-.090	-.229	-.025	-.297	-.028	-.029	-.042
	DGRL [85]	.831	-.088	-.365	-.050	-.402	-.031	-.022	-.026
	PiCANet [39]	.848	-.048	-.175	-.014	-.148	-.005	-.008	-.039
	*ND-avg	.627	-.015	-.066	-.027	-.104	-.000	-.001	-.087
	D-avg	.832	-.075	-.256	-.041	-.282	-.021	-.020	-.037

* Non-deep learning model.

Table 7). For both types of methods, *Natural* is the easiest, which is reasonable since the scenes are typically simple. Though both containing a plunge of objects, *Indoor* is harder than *Urban* as the former often suffers from highly unevenly distributed illuminations and more complex scenes. These experiments also demonstrate the utility of SOD models in real, especially complex, environments is still limited.

• **Additional advantages of deep models.** As shown in Table 7, deep models achieve great improvements on semantic-rich objects (*Human*, *Animal* and *Artifact*), showing the advantages in semantics modeling. This is verified again by their good performance over complex object shapes (*HO*, *OV*, *OC*, *CT*). Deep models also narrow the gap between different scene categories (*Indoor* v.s. *Natural*), suggesting the improved robustness against various backgrounds.

• **Best and worst predictions.** From Table 8, in addition to similar conclusions drawn from Table 7, some unique observations are interesting. For deep methods, the degree of challenges raised by *NatObj* spans a large range; both simplest and hardest samples are contained. Thus future efforts should pay more attention to these hardest samples in *NatObj*. In addition, after considering data distribution bias, *CS* are the most challenging factor for deep models.

5.4 Robustness against General Input Perturbations

The robustness of a model lies in its stability against corrupt inputs. Intuitively, the outputs of a robust SOD model should be repeatable on slightly different images with the same content. On the other hand, the recently emerged adversarial examples, *i.e.* the maliciously constructed inputs that fool the trained models, can degrade the performance

	Original	Gaussian blur		Gaussian noise		Rotation		Gray
		sigma=2	sigma=4	var=0.01	var=0.08	15°	-15°	
Image								
GT								
HS		0.844	0.797	0.791	0.836	0.785	0.808	0.794
DREI		0.846	0.830	0.839	0.844	0.806	0.806	0.849
wCrt		0.866	0.857	0.856	0.841	0.773	0.743	0.806
SRM		0.922	0.851	0.819	0.808	0.700	0.828	0.857
DGRL		0.880	0.848	0.821	0.927	0.714	0.905	0.865
PiCANet		0.945	0.872	0.835	0.924	0.840	0.926	0.890

	Original	Gaussian blur		Gaussian noise		Rotation		Gray
		sigma=2	sigma=4	var=0.01	var=0.08	15°	-15°	
Image								
GT								
HS		0.579	0.655	0.550	0.541	0.573	0.742	0.653
DREI		0.533	0.571	0.537	0.573	0.571	0.688	0.627
wCrt		0.670	0.618	0.627	0.564	0.612	0.578	0.643
SRM		0.951	0.565	0.471	0.731	0.532	0.791	0.896
DGRL		0.927	0.523	0.471	0.645	0.471	0.820	0.888
PiCANet		0.947	0.814	0.471	0.860	0.471	0.851	0.848

Fig. 5. Examples of saliency prediction under various input perturbations. The max F values are denoted using red. See §5.4 for more details.

of deep image classifiers significantly. Current deep SOD models may face a similar challenge. Therefore, in this section, we examine the robustness of SOD models by comparing their outputs over randomly perturbed inputs, such as noisy or blurred images. Then, in §5.5, we will study the robustness to manually designed adversarial examples.

The experimented input perturbations include *Gaussian blur*, *Gaussian noise*, *Rotation*, and *Gray*. For blurring, we use Gaussian blur kernels with sigma of 2 or 4. For noise, we select two variance values, *i.e.*, 0.01 and 0.08, to cover both tiny and medium magnitudes. For rotation, we rotate the images for +15° and -15°, respectively, and cut out the largest box with the original aspect ratio. The gray images are generated using Matlab `rgb2gray` function.

As in §5.3, we include three popular heuristic models [34], [35], [53] and three deep methods [39], [71], [85] in our experiments. Table 9 shows the results. Overall, compared with deep methods, heuristic methods are less sensitive towards input perturbations. The compactness and abstractness of superpixels likely explains much of this effect. Specifically, heuristic methods are rarely affected by *Rotation*, but perform worse for strong *Gaussian blur*, strong *Gaussian noise* and *Gray* effect. Deep methods suffer the most for *Gaussian blur* and strong *Gaussian noise*, which may be caused by the damage of shallow-layer features. Deep methods are relatively robust against *Rotation*, revealing the rotation invariance of DNNs brought by the pooling operation. Interestingly, we further find that, among the three deep models, PiCANet[39] show super robustness against a wide range of input perturbations, including *Gaussian blur*, *Gaussian noise*, and *Rotation*. We attribute this to its effective non-local operation. This reveals effective network designs can improve the robustness to random perturbations.

5.5 Robustness against Manually Designed Input Perturbations

Given the significant concerns with model robustness to random perturbations that have been discussed, this section presents analysis grounded more heavily in robustness against manually designed adversarial perturbations. Modern DNNs are shown surprisingly susceptible to adversarial attacks, where visually imperceptible perturbations would

	Original	Attack SRM	Attack DGRL	Attack PiCANet	Original	Attack SRM	Attack DGRL	Attack PiCANet
Image								
GT								
SRM		0.922	0.480	0.899	0.951	0.588	0.871	0.883
DGRL		0.680	0.861	0.471	0.927	0.883	0.869	0.843
PiCANet		0.945	0.920	0.941	0.947	0.935	0.925	0.920

Fig. 6. Adversarial examples for saliency prediction under adversarial perturbations of different target networks. The perturbations are magnified by 10 for better visualization. Red for max F . See §5.5 for details.

lead to completely different predictions[140]. Though being intensively studied in classification tasks, adversarial attacks in SOD are rarely explored. From a more practical view, SOD has benefited a wide range of applications, including military and security systems (*e.g.*, remote sensing image analysis [141], video surveillance [142], autonomous driving [143]), and commercial projects (*e.g.*, photo editing [19], image and video compression [144]). These applications have always been enticing targets for various attackers such as hackers, criminals, and hostile organizations. Thus studying the robustness of SOD models is crucial for defending these applications against malicious attacks.

In this section, we study the robustness against adversarial attacks and transferability of adversarial examples targeted on different SOD models. Our observations are expected to shed light on adversarial attacks and defenses of SOD, and better understand model vulnerabilities.

5.5.1 Robustness of SOD against Adversarial Attacks

Since SOD can be viewed as a special case of semantic segmentation with two predefined categories, we resort to an adversarial attack algorithm designed for semantic segmentation, *i.e.* *Dense Adversary Generation* (DAG) [145], for measuring the robustness of deep SOD models. We choose three representative deep models, *i.e.*, SRM [71], DGRL[85] and PiCANet[39], to study the robustness against adversarial attacks. The experiment is conducted on the hybrid benchmark introduced in §5.3.

TABLE 10

Results for adversarial attack experiments. $\max F\uparrow$ on the **hybrid benchmark** is presented when exerting adversarial perturbations from different models. Worst with underline. See §5.5 for details.

Attack from	SRM [71]	DGRL [85]	PiCANet [39]
None	.817	.831	.848
SRM [71]	<u>.263</u>	.780	.842
DGRL [85]	.778	<u>.248</u>	.844
PiCANet [39]	.772	.799	<u>.253</u>

Exemplar adversarial cases are shown in Fig. 6. Quantitative results are listed in Table 10. The underlined entries of Table 10 revealed that the three experimented deep SOD models are vulnerable to adversarial perturbations of the inputs. On the other hand, it can be observed by comparing Tables 9 and 10 that these models are relatively more robust to random input perturbations. The differences of the robustness towards these two kinds of perturbations might be interpreted by the the distance from the inputs to the decision boundary in high dimensional space. The intentionally designed adversarial inputs often lie closer to the decision boundary than the random inputs [146], thus can cause pixel-wise misclassification more easily.

5.5.2 Transferability across Networks

Previous researches have revealed that the adversarial perturbations can be transferred across networks, *i.e.* adversarial examples targeted against one model can mislead another model without any modification [147]. Such transferability is widely used for black-box attack against real-world system. To investigate the transferability of the generated perturbations for deep SOD models, we use the adversarial perturbation computed on one SOD model to attack another.

Table 10 shows the results of the experiment to evaluate the transferability among 3 studied models (SRM [71], DGRL [85] and PiCANet [39]). While the DAG attack leads to severe performance drops for the targeted model (see the diagonal), it causes much less degradation to other models. This may be because that the gradient directions of different models are orthogonal to each other [148], thus the gradient-based attack in the experiment transfers poorly to other non-targeted models. However, adversarial images generated from an ensemble of multiple models might generate non-targeted adversarial instances with better transferability [148], which shall be a great threat for deep SOD models.

5.6 Cross-Dataset Generalization Evaluation

Datasets are responsible for much of recent progress in visual saliency modeling, not just as source for training deep models, but also as a means for measuring and comparing performance. Datasets are collected with the goal of representing the visual world, summarizing the algorithm as a single benchmark performance number. A concern thus comes into view: it is necessary to evaluate how well a particular dataset represent the real world. Or more specifically, quantitatively measuring the dataset’s generalization ability. Unfortunately, previous studies [43] are largely restricted to a quite limited view of center bias. Here, we follow [149] to assess how general SOD datasets are. We study the

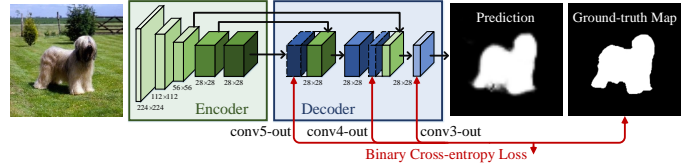


Fig. 7. Network architecture of the SOD model used in cross-dataset generalization evaluation. See §5.6 for more detailed descriptions.

TABLE 11

Results for cross-dataset generalization experiment. $\max F\uparrow$ for saliency prediction when training on one dataset (rows) and testing on another (columns). “Self” refers to training and testing on the same dataset (same as diagonal). “Mean Others” indicates average performance on all except self. See §5.6 for details.

Train on:	Test on:	MSRA-10K [107]	ECSSD [55]	DUT-OMRON [56]	HKU-IS [26]	DUTS [97]	SOC [130]	Self	Mean others	Percent drop↓
MSRA10K [107]		.875	.818	.660	.849	.671	.617	.875	.723	17%
ECSSD [55]		.844	.831	.630	.833	.646	.616	.831	.714	14%
DUT-OMRON [56]		.795	.752	.673	.779	.623	.567	.673	.703	-5%
HKU-IS [26]		.857	.838	.695	.880	.719	.639	.880	.750	15%
DUTS [97]		.857	.834	.647	.860	.665	.654	.665	.770	-16%
SOC [130]		.700	.670	.517	.666	.514	.593	.593	.613	-3%
Mean others		.821	.791	.637	.811	.640	.614	-	-	-

generalization and hardness of several main-stream SOD datasets by performing cross-dataset analysis, *i.e.*, training on one dataset, and testing on the others. Our experiments are expected to stimulate discussion in the community regarding this very essential, but largely neglected issue.

We first train a typical SOD model on one dataset, and then explore how well it generalizes on a representative set of other datasets, compared with its performance on the “native” test set. Specifically, we implement the typical SOD model as a bottom-up/top-down structure, that has been the most standard and popular SOD architecture in recent years, and is the basis of currently top-performing models [82], [93], [101], [102]. As shown in Fig. 7, the encoder part is borrowed from VGG16 [150], and the decoder part consists of three convolutional layers to gradually refine the saliency prediction. We pick six representative datasets [26], [55], [56], [97], [107], [130]. For each dataset, we train the SOD model with 800 randomly selected training images and test it on 200 other validation images. Please note that 1,000 is the maximum possible total number considering the size of the smallest selected dataset, ECSSD [55].

Table 11 summarizes the results of cross-dataset generalization, measured by $\max F$. Each column corresponds to the performance when training on all the datasets respectively and testing on one dataset. Each row corresponds to training on one dataset and testing on all the datasets. Note that since our training/testing protocol is different from the one used in benchmarks mentioned in previous sections, the actual performance numbers are not meaningful. Rather, it is the relative performance difference that matters. Not surprisingly, we observe that the best results are achieved when training and testing on the same dataset. By looking at the numbers across each column, we can determine how easy a dataset is for the other datasets. By looking at the numbers across one row, we can determine how good a dataset is at generalizing to the others. We find that SOC [130] is the most difficult dataset (lowest column

Mean others 0.614). MSRA10K [107] appears to be the easiest dataset (highest column *Mean others* 0.811), and generalizes the worst (highest row *Percent drop* 17%). DUTS [97] is shown to have the best generalization ability (lowest row *Percent drop* -16%).

Based on these analyses, we would make the following recommendations for SOD datasets: 1) For training deep models, DUTS [97] is a good choice because it has the best generalizability. 2) For testing, SOC [130] would be a proper reference to assess the worst-case performances, since it is the hardest dataset. DUT-OMRON [56] and DUTS-test [97] should be better considered as they are also very hard.

6 MORE DISCUSSIONS

The previous systematic review and empirical studies characterize the models (§2), datasets (§3), metrics (§4), and challenges (§5) of deep SOD methods. Here we further posit active research directions, and outline several open issues.

6.1 Model Design

Based on the review of deep SOD network architectures in §2.1 as well as recent advances in related fields, we here discuss several essential directions for SOD model design.

- **Network topology.** Network topology determines the within-network information flow that directly affects model capacity and training difficulty, thus influencing the best possible performance. To figure out an effective network topology for SOD, diverse architectures have been explored (§2.1), such as multi-stream networks, side-out fusion networks, as well as bottom-up/top-down networks. However, all these network architectures are hand-designed. Thus a promising direction is to resort to *Automated Machine Learning* (AutoML) algorithms, such as *Neural Architecture Search* [151], for automatically searching for the best performing SOD network topology.
- **Loss function.** Most deep SOD methods are trained with the standard binary cross-entropy loss, which may fail to fully capture the quality factors for SOD task. Only a few efforts have been made to derive losses from SOD evaluation metrics [87]. Thus it is worth exploring more effective SOD loss functions, such as mean intersection-over-union loss [152] and affinity field matching loss [153].
- **Adaptive computation.** Currently all the deep SOD models are fixed feed-forward structures. However, most parameters model high-level features that, in contrast to low-level and many mid-level concepts, cannot be broadly shared across categories/scenes. So, we would like to ask the following question: what if a SOD model could execute directly certain layers that can best explain the saliency patterns in the given scene? To answer this, one can leverage adaptive computation techniques [154], [155] to vary the amount of computation on-the-fly, *i.e.*, selectively activating part of the network in an input-dependent fashion. This could bring a better trade-off between network depth and computation cost. On the other hand, adapting inference pathways for different inputs would provide finer-grained discriminative ability for various attributes. Therefore, exploring dynamic network structures in SOD is promising for improving both efficiency and effectiveness.

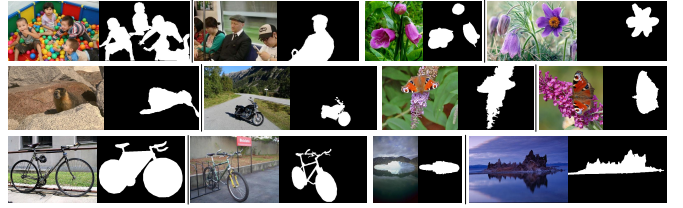


Fig. 8. Examples for annotation inconsistency. Each row shows two exemplar image pairs. See §6.2 for more detailed descriptions.

6.2 Data Collection

Previous introductions (§3) and analyses (§5.3 and §5.6) on current SOD datasets reveal several factors that are essential for dataset collection in future.

- **Annotation inconsistency.** Though existing SOD datasets play a critical role in training and evaluating modern SOD models, annotation inconsistencies among different SOD datasets are relatively neglected in the community. The inconsistencies are mainly caused by separate subjects and rules/conditions during dataset annotation (see Fig. 8). To ease annotation burden, most current SOD datasets only let a few human annotators to directly identify the salient objects, instead of considering real human eye fixation behavior. Maintaining annotation consistency among newly collected datasets is a non-negligible consideration.
- **Coarse v.s. fine annotation.** Modern SOD datasets are all with pixel-wise annotations, which greatly boosts the performance of deep SOD models. However, pixel-wise groundtruths are very costly to collect considering the complex object boundaries and the intense data requirement. Actually, the annotation qualities of different datasets are different (see bicycles in Fig. 8). Finer labels are believed to be essential for high-quality saliency prediction, but usually need more time to collect. Thus, given a limited budget, how to find the optimal annotation strategy is an open and unsolved problem. Some works studied the relationship between label quality and model performance in semantic segmentation [156], which points out a possible research direction for SOD dataset collection. In addition, current SOD models typically assume the annotations are perfect. Thus it is also of value in exploring robust SOD models that can learn saliency patterns from imperfectly annotated data.
- **Domain-specific SOD datasets.** SOD has been shown potential in a wide range of applications such as autonomous vehicles, video games, medical image processing, *etc.* Due to different visual appearances and semantic components, saliency mechanisms in these applications should be quite different from that in conventional natural images. Thus, collecting domain-specific datasets might benefit the application of SOD in certain scenarios, as observed in FP for crowds [157], webpages [158] or driving [159], and better connect SOD to biological top-down visual attention mechanism and human mental state.

6.3 Saliency Ranking and Relative Saliency

Current algorithms seems over-focus on directly regressing the saliency map to pursue a high benchmarking number, while neglecting that the absolute magnitude of values in a saliency map might be considered less important than relative saliency values among objects [108]. Though the relative value/rank order is rarely considered in the context of

benchmarking metrics (only except [79]), it is fundamentally crucial for better modeling human visual attention behavior, which is in essence a selection process that centers our attention on certain important elements of the surrounding while blends other relatively unimportant things into the background. This not only hints at one shortcoming of existing benchmarking paradigms and data collection, but also reveals a common limitation of current methods. Current arts are short at reasoning about the relative importance of objects, such as discovering the most important person from a crowded room. This is also evidenced by the experiments in §5.3, which show that deep models face great difficulties in complex (*CS*), indoor (*Indoor*) or multi-object (*MO*) scenes. In other words, deep models, though being good at semantics modeling, require higher-level image understanding. Exploring more powerful network designs that explicitly reason the relative saliency and revisiting classic cognitive theories are both promising direction to overcome this issue.

6.4 Link SOD to Visual Fixations

The strong correlation between eye movements (implicit saliency) and explicit object saliency has been explored in history [43], [108], [160]–[162]. However, despite the deep connections between the problems of FP and SOD, there exists a significant isolation between major computational models of the two types; only a few SOD models consider the two tasks simultaneously [72], [87], [96]. This is mainly due to the overemphasis of the task-specific setting of SOD and the design bias of current SOD datasets, which overlooks the connection to eye fixations during data annotation. As stated in [108], such dataset design bias does not only create the disconcerting disconnection between FP and SOD, but also further misleads the algorithm designing. Exploring classic visual attention theories in SOD is a promising and crucial direction which can make SOD models more consistent with visual processing of human visual system and gain better explainability. In addition, the ultimate goal of visual saliency modeling is to understand the underlying rationale of visual attention mechanism. However, with the gradually improved focus on exploring more powerful neural network architectures and beating the latest benchmark numbers on the datasets, have we perhaps lost sight of the original purpose? The solution of these problems requires dense collaborations of FP and SOD communities.

6.5 Learning SOD in a Un-/Weakly-Supervised Manner

Deep SOD methods are typically trained in a fully-supervised manner with a plethora of fine-annotated pixel-wise ground-truths. However, it is highly-costly and time-consuming to construct a large-scale, well-annotated SOD dataset. Though a few efforts have been made, *i.e.*, leveraging category-level labels [68], [69], [97] or pseudo pixel-wise annotations [67], [81], [83], [98], [99], there is still a notable gap with the fully-supervised counterparts. In addition, our humans usually learn with little even no supervision. In addition, the ultimate goal of visual saliency modeling is to understand the visual attention mechanism, which is a central ability of our perception system. Thus, learning SOD in an un-/weakly-supervised manner is of great value in both research and real-world application. And it helps

understand which factors that truly drive our attention mechanism and saliency pattern understanding. Given the massive number of algorithmic breakthroughs over the past few years, we can expect a flurry of innovation towards this promising direction.

6.6 Pre-training with Self-Supervised Visual Features

Current deep SOD methods are typically built on ImageNet-pretrained networks, and fine-tuned on SOD datasets. It is believed that the parameters trained on ImageNet can serve as a good starting point to accelerate the convergence of training and avoiding overfitting on the smaller scale SOD datasets. Besides pre-training deep SOD models on the *de facto* dataset, ImageNet, another choice is to leverage self-supervised learning techniques [163] to learn effective visual features from a vast amount of unlabeled images/videos. The visual features can be learned through various pretext tasks like image inpainting [164], colorization [165], clustering [166], *etc.*, and can be generalized to other vision tasks. Fine-tuning the SOD models on parameters trained from self-supervised learning is promising to yield better performance compared with the ImageNet initialization.

6.7 Efficient SOD for Real-World Application

Current top-leading deep SOD models are designed to be complicated in order to achieve increased learning capacity and improved performance. However, more ingenious and light-weighted architectures are required to fulfill the requirements of mobile and embedded applications, such as robotics, autonomous driving, augmented reality, *etc.* The degradation of accuracy and generalization ability caused by model scale deduction is desired to be minimum. To facilitate the application of SOD in real-world scenarios, it is considerable to utilize model compression [167] or knowledge distillation [168], [169] techniques to develop compact and fast SOD models with competitive performance. Such compression techniques have already been shown effective in improving generalization ability and alleviating underfitting for training efficient object detection models [170].

7 CONCLUSION

In this paper we present, to the best of our knowledge, the first comprehensive review of SOD which focuses on deep learning techniques. We first provide novel testimonies for categorizing deep SOD models from several distinct perspectives, including network architecture, level of supervision, *etc.* We then cover the contemporary literature of popular SOD datasets and evaluation criteria, providing a thorough performance benchmarking of major SOD methods and offering recommendations of several datasets and metrics to consistently assess SOD models. Next, we consider several previously under-explored issues relevant to benchmarking and baselines with novel efforts. In particular, we study the strengths and weaknesses of deep and non-deep SOD models by compiling and annotating a new dataset and evaluating several representative models on it, which reveals promising directions for future efforts. We also study the robustness of SOD methods by analyzing the effects of various perturbations on the final performance. Moreover, for the first time in the field, we investigate the

robustness of deep SOD models w.r.t. maliciously designed adversarial perturbations and the transferability of these adversarial examples, which provides baselines for future research. In addition, we analyze the generalization and difficulty of existing SOD datasets through a cross-dataset generalization study, and quantitatively reveal the dataset bias. We finally look through several open issues and challenges of SOD in deep learning era, providing insightful discussions and identifying a number of potentially fruitful directions forward.

In conclusion, SOD has been approached with notable progress thanks to the striking development of deep learning techniques, yet there are still under-explored problems on achieving more efficient designing, training, and inferring for both academic research and real-world application. We expect this survey to provide an effective way to understand state-of-the-arts and, more importantly, insights for future exploration in SOD.

REFERENCES

- [1] J.-Y. Zhu, J. Wu, Y. Xu, E. Chang, and Z. Tu, "Unsupervised object class discovery via saliency-guided multiple class learning," *IEEE Trans. Pattern Anal. Mach. Intell.*, vol. 37, no. 4, pp. 862–875, 2015.
- [2] F. Zhang, B. Du, and L. Zhang, "Saliency-guided unsupervised feature learning for scene classification," *IEEE Trans. Geosci. Remote Sens.*, vol. 53, no. 4, pp. 2175–2184, 2015.
- [3] K. Xu, J. Ba, R. Kiros, K. Cho, A. Courville, R. Salakhudinov, R. Zemel, and Y. Bengio, "Show, attend and tell: Neural image caption generation with visual attention," in *Proc. ACM Int. Conf. Mach. Learn.*, 2015, pp. 2048–2057.
- [4] H. Fang, S. Gupta, F. Iandola, R. K. Srivastava, L. Deng, P. Dollár, J. Gao, X. He, M. Mitchell, J. C. Platt *et al.*, "From captions to visual concepts and back," in *Proc. IEEE Conf. Comput. Vis. Pattern Recognit.*, 2015, pp. 1473–1482.
- [5] A. Das, H. Agrawal, L. Zitnick, D. Parikh, and D. Batra, "Human attention in visual question answering: Do humans and deep networks look at the same regions?" *Computer Vision and Image Understanding*, vol. 163, pp. 90–100, 2017.
- [6] Z. Ren, S. Gao, L.-T. Chia, and I. W.-H. Tsang, "Region-based saliency detection and its application in object recognition," *IEEE Trans. Circuits Syst. Video Technol.*, vol. 24, no. 5, pp. 769–779, 2014.
- [7] D. Zhang, D. Meng, L. Zhao, and J. Han, "Bridging saliency detection to weakly supervised object detection based on self-paced curriculum learning," in *International Joint Conferences on Artificial Intelligence*, 2016.
- [8] W. Wang, J. Shen, R. Yang, and F. Porikli, "Saliency-aware video object segmentation," *IEEE Trans. Pattern Anal. Mach. Intell.*, vol. 40, no. 1, pp. 20–33, 2018.
- [9] H. Song, W. Wang, S. Zhao, J. Shen, and K.-M. Lam, "Pyramid dilated deeper convlstm for video salient object detection," in *Proc. Eur. Conf. Comput. Vis.*, 2018.
- [10] Y. Wei, J. Feng, X. Liang, M.-M. Cheng, Y. Zhao, and S. Yan, "Object region mining with adversarial erasing: A simple classification to semantic segmentation approach," in *Proc. IEEE Conf. Comput. Vis. Pattern Recognit.*, 2017.
- [11] Y. Wei, X. Liang, Y. Chen, X. Shen, M.-M. Cheng, J. Feng, Y. Zhao, and S. Yan, "STC: A simple to complex framework for weakly-supervised semantic segmentation," *IEEE Trans. Pattern Anal. Mach. Intell.*, vol. 39, no. 11, pp. 2314–2320, 2017.
- [12] X. Wang, S. You, X. Li, and H. Ma, "Weakly-supervised semantic segmentation by iteratively mining common object features," in *Proc. IEEE Conf. Comput. Vis. Pattern Recognit.*, 2018.
- [13] R. Zhao, W. Ouyang, and X. Wang, "Unsupervised salience learning for person re-identification," in *Proc. IEEE Conf. Comput. Vis. Pattern Recognit.*, 2013, pp. 3586–3593.
- [14] S. Bi, G. Li, and Y. Yu, "Person re-identification using multiple experts with random subspaces," *Journal of Image and Graphics*, vol. 2, no. 2, 2014.
- [15] Y.-F. Ma, L. Lu, H.-J. Zhang, and M. Li, "A user attention model for video summarization," in *Proc. ACM Int. Conf. Multimedia*, 2002, pp. 533–542.
- [16] D. Simakov, Y. Caspi, E. Shechtman, and M. Irani, "Summarizing visual data using bidirectional similarity," in *Proc. IEEE Conf. Comput. Vis. Pattern Recognit.*, 2008, pp. 1–8.
- [17] J. Han, E. J. Pauwels, and P. De Zeeuw, "Fast saliency-aware multi-modality image fusion," *Neurocomputing*, vol. 111, pp. 70–80, 2013.
- [18] P. L. Rosin and Y.-K. Lai, "Artistic minimal rendering with lines and blocks," *Graphical Models*, vol. 75, no. 4, pp. 208–229, 2013.
- [19] W. Wang, J. Shen, and H. Ling, "A deep network solution for attention and aesthetics aware photo cropping," *IEEE Trans. Pattern Anal. Mach. Intell.*, 2018.
- [20] S. Avidan and A. Shamir, "Seam carving for content-aware image resizing," in *ACM Trans. Graph.*, vol. 26, no. 3, 2007, p. 10.
- [21] J. Sun and H. Ling, "Scale and object aware image retargeting for thumbnail browsing," in *Proc. IEEE Int. Conf. Comput. Vis.*, 2011.
- [22] Y. Sugano, Y. Matsushita, and Y. Sato, "Calibration-free gaze sensing using saliency maps," in *Proc. IEEE Conf. Comput. Vis. Pattern Recognit.*, 2010, pp. 2667–2674.
- [23] A. Borji and L. Itti, "Defending yarbush: Eye movements reveal observers' task," *Journal of Vision*, vol. 14, no. 3, pp. 29–29, 2014.
- [24] A. Karpathy, S. Miller, and L. Fei-Fei, "Object discovery in 3d scenes via shape analysis," in *Proc. IEEE Conf. Robot. Autom.*, 2013, pp. 2088–2095.
- [25] S. Frintrop, G. M. García, and A. B. Cremers, "A cognitive approach for object discovery," in *Proc. IEEE Conf. Comput. Vis. Pattern Recognit.*, 2014, pp. 2329–2334.
- [26] G. Li and Y. Yu, "Visual saliency based on multiscale deep features," in *Proc. IEEE Conf. Comput. Vis. Pattern Recognit.*, 2015, pp. 5455–5463.
- [27] L. Wang, H. Lu, X. Ruan, and M.-H. Yang, "Deep networks for saliency detection via local estimation and global search," in *Proc. IEEE Conf. Comput. Vis. Pattern Recognit.*, 2015, pp. 3183–3192.
- [28] R. Zhao, W. Ouyang, H. Li, and X. Wang, "Saliency detection by multi-context deep learning," in *Proc. IEEE Conf. Comput. Vis. Pattern Recognit.*, 2015, pp. 1265–1274.
- [29] T. Liu, J. Sun, N.-N. Zheng, X. Tang, and H.-Y. Shum, "Learning to detect a salient object," in *Proc. IEEE Conf. Comput. Vis. Pattern Recognit.*, 2007, pp. 1–8.
- [30] R. Achanta, S. Hemami, F. Estrada, and S. Susstrunk, "Frequency-tuned salient region detection," in *Proc. IEEE Conf. Comput. Vis. Pattern Recognit.*, 2009, pp. 1597–1604.
- [31] M.-M. Cheng, G.-X. Zhang, N. J. Mitra, X. Huang, and S.-M. Hu, "Global contrast based salient region detection," *Proc. IEEE Conf. Comput. Vis. Pattern Recognit.*, 2011.
- [32] F. Perazzi, P. Krähenbühl, Y. Pritch, and A. Hornung, "Saliency filters: Contrast based filtering for salient region detection," in *Proc. IEEE Conf. Comput. Vis. Pattern Recognit.*, 2012, pp. 733–740.
- [33] J. Wang, H. Jiang, Z. Yuan, M.-M. Cheng, X. Hu, and N. Zheng, "Salient object detection: A discriminative regional feature integration approach," *Int. J. Comput. Vis.*, vol. 123, no. 2, pp. 251–268, 2017.
- [34] Q. Yan, L. Xu, J. Shi, and J. Jia, "Hierarchical saliency detection," in *Proc. IEEE Conf. Comput. Vis. Pattern Recognit.*, 2013, pp. 1155–1162.
- [35] W. Zhu, S. Liang, Y. Wei, and J. Sun, "Saliency optimization from robust background detection," in *Proc. IEEE Conf. Comput. Vis. Pattern Recognit.*, 2014, pp. 2814–2821.
- [36] J. Zhang, S. Sclaroff, Z. Lin, X. Shen, B. Price, and R. Mech, "Unconstrained salient object detection via proposal subset optimization," in *Proc. IEEE Conf. Comput. Vis. Pattern Recognit.*, 2016, pp. 5733–5742.
- [37] N. Liu and J. Han, "DHSNet: Deep hierarchical saliency network for salient object detection," in *Proc. IEEE Conf. Comput. Vis. Pattern Recognit.*, 2016, pp. 678–686.
- [38] Q. Hou, M.-M. Cheng, X. Hu, A. Borji, Z. Tu, and P. Torr, "Deeply supervised salient object detection with short connections," in *Proc. IEEE Conf. Comput. Vis. Pattern Recognit.*, 2017, pp. 3203–3212.
- [39] N. Liu, J. Han, and M.-H. Yang, "Picanet: Learning pixel-wise contextual attention for saliency detection," in *Proc. IEEE Conf. Comput. Vis. Pattern Recognit.*, 2018, pp. 3089–3098.
- [40] Y. Liu, Q. Zhang, D. Zhang, and J. Han, "Employing deep part-object relationships for salient object detection," in *Proc. IEEE Int. Conf. Comput. Vis.*, 2019, pp. 1232–1241.
- [41] Q. Qi, S. Zhao, J. Shen, and K.-M. Lam, "Multi-scale capsule attention-based salient object detection with multi-crossed layer

- connections," in *IEEE International Conference on Multimedia and Expo*, 2019, pp. 1762–1767.
- [42] A. Borji and L. Itti, "State-of-the-art in visual attention modeling," *IEEE Trans. Pattern Anal. Mach. Intell.*, vol. 35, no. 1, pp. 185–207, 2013.
- [43] A. Borji, M.-M. Cheng, H. Jiang, and J. Li, "Salient object detection: A benchmark," *IEEE Trans. Image Process.*, vol. 24, no. 12, pp. 5706–5722, 2015.
- [44] T. V. Nguyen, Q. Zhao, and S. Yan, "Attentive systems: A survey," *Int. J. Comput. Vis.*, vol. 126, no. 1, pp. 86–110, 2018.
- [45] D. Zhang, H. Fu, J. Han, A. Borji, and X. Li, "A review of co-saliency detection algorithms: fundamentals, applications, and challenges," *ACM Trans. Intell. Syst. Technol.*, vol. 9, no. 4, p. 38, 2018.
- [46] R. Cong, J. Lei, H. Fu, M.-M. Cheng, W. Lin, and Q. Huang, "Review of visual saliency detection with comprehensive information," *IEEE Trans. Circuits Syst. Video Technol.*, 2018.
- [47] J. Han, D. Zhang, G. Cheng, N. Liu, and D. Xu, "Advanced deep-learning techniques for salient and category-specific object detection: a survey," *IEEE Signal Processing Magazine*, vol. 35, no. 1, pp. 84–100, 2018.
- [48] A. Borji, "Saliency prediction in the deep learning era: Successes and limitations," *IEEE Trans. Pattern Anal. Mach. Intell.*, 2019.
- [49] A. Borji, M.-M. Cheng, Q. Hou, H. Jiang, and J. Li, "Salient object detection: A survey," *Computational Visual Media*, pp. 1–34, 2019.
- [50] A. M. Treisman and G. Gelade, "A feature-integration theory of attention," *Cognitive psychology*, vol. 12, no. 1, pp. 97–136, 1980.
- [51] C. Koch and S. Ullman, "Shifts in selective visual attention: Towards the underlying neural circuitry," *Human neurobiology*, vol. 4, no. 4, p. 219, 1985.
- [52] L. Itti, C. Koch, and E. Niebur, "A model of saliency-based visual attention for rapid scene analysis," *IEEE Trans. Pattern Anal. Mach. Intell.*, vol. 20, no. 11, pp. 1254–1259, 1998.
- [53] H. Jiang, J. Wang, Z. Yuan, Y. Wu, N. Zheng, and S. Li, "Salient object detection: A discriminative regional feature integration approach," in *Proc. IEEE Conf. Comput. Vis. Pattern Recognit.*, 2013, pp. 2083–2090.
- [54] Y. Wei, F. Wen, W. Zhu, and J. Sun, "Geodesic saliency using background priors," *Proc. Eur. Conf. Comput. Vis.*, pp. 29–42, 2012.
- [55] J. Shi, Q. Yan, L. Xu, and J. Jia, "Hierarchical image saliency detection on extended cssd," *IEEE Trans. Pattern Anal. Mach. Intell.*, vol. 38, no. 4, pp. 717–729, 2015.
- [56] C. Yang, L. Zhang, H. Lu, X. Ruan, and M. H. Yang, "Saliency detection via graph-based manifold ranking," in *Proc. IEEE Conf. Comput. Vis. Pattern Recognit.*, 2013, pp. 3166–3173.
- [57] W. Wang, J. Shen, L. Shao, and F. Porikli, "Correspondence driven saliency transfer," *IEEE Trans. Image Process.*, vol. 25, no. 11, pp. 5025–5034, 2016.
- [58] F. Guo, W. Wang, J. Shen, L. Shao, J. Yang, D. Tao, and Y. Y. Tang, "Video saliency detection using object proposals," *IEEE Trans. Cybernetics*, 2017.
- [59] G. E. Hinton, A. Krizhevsky, and S. D. Wang, "Transforming auto-encoders," in *Proc. Int. Conf. Artificial Neural Netw.*, 2011, pp. 44–51.
- [60] G. Lee, Y.-W. Tai, and J. Kim, "Deep saliency with encoded low level distance map and high level features," in *Proc. IEEE Conf. Comput. Vis. Pattern Recognit.*, 2016, pp. 660–668.
- [61] S. He, R. W. Lau, W. Liu, Z. Huang, and Q. Yang, "Supercnn: A superpixelwise convolutional neural network for salient object detection," *Int. J. Comput. Vis.*, vol. 115, no. 3, pp. 330–344, 2015.
- [62] J. Kim and V. Pavlovic, "A shape-based approach for salient object detection using deep learning," in *Proc. Eur. Conf. Comput. Vis.*, 2016, pp. 455–470.
- [63] L. Wang, L. Wang, H. Lu, P. Zhang, and X. Ruan, "Saliency detection with recurrent fully convolutional networks," in *Proc. Eur. Conf. Comput. Vis.*, 2016, pp. 825–841.
- [64] J. Kuen, Z. Wang, and G. Wang, "Recurrent attentional networks for saliency detection," in *Proc. IEEE Conf. Comput. Vis. Pattern Recognit.*, 2016, pp. 3668–3677.
- [65] P. Hu, B. Shuai, J. Liu, and G. Wang, "Deep level sets for salient object detection," in *Proc. IEEE Conf. Comput. Vis. Pattern Recognit.*, 2017, pp. 540–549.
- [66] P. Zhang, D. Zhang, H. Lu, H. Wang, and B. Yin, "Learning uncertain convolutional features for accurate saliency detection," in *Proc. IEEE Int. Conf. Comput. Vis.*, 2017, pp. 212–221.
- [67] J. Zhang, T. Zhang, Y. Dai, M. Harandi, and R. Hartley, "Deep unsupervised saliency detection: A multiple noisy labeling perspective," in *Proc. IEEE Conf. Comput. Vis. Pattern Recognit.*, 2018, pp. 9029–9038.
- [68] C. Cao, Y. Hunag, Z. Wang, L. Wang, N. Xu, and T. Tan, "Lateral inhibition-inspired convolutional neural network for visual attention and saliency detection," in *AAAI Conference on Artificial Intelligence*, 2018.
- [69] B. Li, Z. Sun, and Y. Guo, "Supervae: Superpixelwise variational autoencoder for salient object detection," in *AAAI Conference on Artificial Intelligence*, 2019, pp. 8569–8576.
- [70] G. Li, Y. Xie, L. Lin, and Y. Yu, "Instance-level salient object segmentation," in *Proc. IEEE Conf. Comput. Vis. Pattern Recognit.*, 2017, pp. 247–256.
- [71] T. Wang, A. Borji, L. Zhang, P. Zhang, and H. Lu, "A stagewise refinement model for detecting salient objects in images," in *Proc. IEEE Int. Conf. Comput. Vis.*, 2017, pp. 4039–4048.
- [72] X. Chen, A. Zheng, J. Li, and F. Lu, "Look, perceive and segment: Finding the salient objects in images via two-stream fixation-semantic CNNs," in *Proc. IEEE Int. Conf. Comput. Vis.*, 2017, pp. 1050–1058.
- [73] Y. Zeng, P. Zhang, J. Zhang, Z. Lin, and H. Lu, "Towards high-resolution salient object detection," in *Proc. IEEE Int. Conf. Comput. Vis.*, 2019, pp. 7234–7243.
- [74] Y. Zhuge, Y. Zeng, and H. Lu, "Deep embedding features for salient object detection," in *AAAI Conference on Artificial Intelligence*, vol. 33, 2019, pp. 9340–9347.
- [75] Z. Luo, A. Mishra, A. Achkar, J. Eichel, S. Li, and P.-M. Jodoin, "Non-local deep features for salient object detection," in *Proc. IEEE Conf. Comput. Vis. Pattern Recognit.*, 2017, pp. 6593–6601.
- [76] P. Zhang, D. Wang, H. Lu, H. Wang, and X. Ruan, "Amulet: Aggregating multi-level convolutional features for salient object detection," in *Proc. IEEE Int. Conf. Comput. Vis.*, 2017, pp. 202–211.
- [77] S. He, J. Jiao, X. Zhang, G. Han, and R. W. Lau, "Delving into salient object subitizing and detection," in *Proc. IEEE Int. Conf. Comput. Vis.*, 2017, pp. 1059–1067.
- [78] X. Hu, L. Zhu, J. Qin, C.-W. Fu, and P.-A. Heng, "Recurrently aggregating deep features for salient object detection," in *AAAI Conference on Artificial Intelligence*, 2018.
- [79] M. Amirul Islam, M. Kalash, and N. D. B. Bruce, "Revisiting salient object detection: Simultaneous detection, ranking, and subitizing of multiple salient objects," in *Proc. IEEE Conf. Comput. Vis. Pattern Recognit.*, 2018.
- [80] Z. Wu, L. Su, and Q. Huang, "Cascaded partial decoder for fast and accurate salient object detection," in *Proc. IEEE Conf. Comput. Vis. Pattern Recognit.*, 2019, pp. 3907–3916.
- [81] Y. Zeng, Y. Zhuge, H. Lu, L. Zhang, M. Qian, and Y. Yu, "Multi-source weak supervision for saliency detection," in *Proc. IEEE Conf. Comput. Vis. Pattern Recognit.*, 2019, pp. 6074–6083.
- [82] J.-X. Zhao, J.-J. Liu, D.-P. Fan, Y. Cao, J. Yang, and M.-M. Cheng, "Egnet: Edge guidance network for salient object detection," in *Proc. IEEE Int. Conf. Comput. Vis.*, 2019, pp. 8779–8788.
- [83] D. Zhang, J. Han, and Y. Zhang, "Supervision by fusion: Towards unsupervised learning of deep salient object detector," in *Proc. IEEE Int. Conf. Comput. Vis.*, vol. 1, no. 2, 2017, p. 3.
- [84] L. Zhang, J. Dai, H. Lu, Y. He, and G. Wang, "A bi-directional message passing model for salient object detection," in *Proc. IEEE Conf. Comput. Vis. Pattern Recognit.*, 2018, pp. 1741–1750.
- [85] T. Wang, L. Zhang, S. Wang, H. Lu, G. Yang, X. Ruan, and A. Borji, "Detect globally, refine locally: A novel approach to saliency detection," in *Proc. IEEE Conf. Comput. Vis. Pattern Recognit.*, 2018, pp. 3127–3135.
- [86] X. Zhang, T. Wang, J. Qi, H. Lu, and G. Wang, "Progressive attention guided recurrent network for salient object detection," in *Proc. IEEE Conf. Comput. Vis. Pattern Recognit.*, 2018, pp. 714–722.
- [87] W. Wang, J. Shen, X. Dong, and A. Borji, "Salient object detection driven by fixation prediction," in *Proc. IEEE Conf. Comput. Vis. Pattern Recognit.*, 2018, pp. 1171–1720.
- [88] S. Chen, X. Tan, B. Wang, and X. Hu, "Reverse attention for salient object detection," in *Proc. Eur. Conf. Comput. Vis.*, 2018, pp. 236–252.
- [89] M. Feng, H. Lu, and E. Ding, "Attentive feedback network for boundary-aware salient object detection," in *Proc. IEEE Conf. Comput. Vis. Pattern Recognit.*, 2019, pp. 1623–1632.
- [90] X. Qin, Z. Zhang, C. Huang, C. Gao, M. Dehghan, and M. Jagersand, "Basnet: Boundary-aware salient object detection," in *Proc. IEEE Conf. Comput. Vis. Pattern Recognit.*, 2019, pp. 7479–7489.

- [91] R. Wu, M. Feng, W. Guan, D. Wang, H. Lu, and E. Ding, "A mutual learning method for salient object detection with intertwined multi-supervision," in *Proc. IEEE Conf. Comput. Vis. Pattern Recognit.*, 2019, pp. 8150–8159.
- [92] W. Wang, S. Zhao, J. Shen, S. C. Hoi, and A. Borji, "Salient object detection with pyramid attention and salient edges," in *Proc. IEEE Conf. Comput. Vis. Pattern Recognit.*, 2019, pp. 1448–1457.
- [93] J.-J. Liu, Q. Hou, M.-M. Cheng, J. Feng, and J. Jiang, "A simple pooling-based design for real-time salient object detection," in *Proc. IEEE Conf. Comput. Vis. Pattern Recognit.*, 2019, pp. 3917–3926.
- [94] W. Wang, J. Shen, M.-M. Cheng, and L. Shao, "An iterative and cooperative top-down and bottom-up inference network for salient object detection," in *Proc. IEEE Conf. Comput. Vis. Pattern Recognit.*, 2019, pp. 5968–5977.
- [95] Y. Xu, D. Xu, X. Hong, W. Ouyang, R. Ji, M. Xu, and G. Zhao, "Structured modeling of joint deep feature and prediction refinement for salient object detection," in *Proc. IEEE Int. Conf. Comput. Vis.*, 2019, pp. 3789–3798.
- [96] S. S. Kruthiventi, V. Gudisa, J. H. Dholakiya, and R. Venkatesh Babu, "Saliency unified: A deep architecture for simultaneous eye fixation prediction and salient object segmentation," in *Proc. IEEE Conf. Comput. Vis. Pattern Recognit.*, 2016, pp. 5781–5790.
- [97] L. Wang, H. Lu, Y. Wang, M. Feng, D. Wang, B. Yin, and X. Ruan, "Learning to detect salient objects with image-level supervision," in *Proc. IEEE Conf. Comput. Vis. Pattern Recognit.*, 2017.
- [98] G. Li, Y. Xie, and L. Lin, "Weakly supervised salient object detection using image labels," in *AAAI Conference on Artificial Intelligence*, 2018.
- [99] X. Li, F. Yang, H. Cheng, W. Liu, and D. Shen, "Contour knowledge transfer for salient object detection," in *Proc. Eur. Conf. Comput. Vis.*, 2018, pp. 370–385.
- [100] L. Zhang, J. Zhang, Z. Lin, H. Lu, and Y. He, "Capsal: Leveraging captioning to boost semantics for salient object detection," in *Proc. IEEE Conf. Comput. Vis. Pattern Recognit.*, 2019, pp. 6024–6033.
- [101] J. Su, J. Li, Y. Zhang, C. Xia, and Y. Tian, "Selectivity or invariance: Boundary-aware salient object detection," in *Proc. IEEE Int. Conf. Comput. Vis.*, 2019, pp. 3799–3808.
- [102] Z. Wu, L. Su, and Q. Huang, "Stacked cross refinement network for edge-aware salient object detection," in *Proc. IEEE Int. Conf. Comput. Vis.*, 2019, pp. 7264–7273.
- [103] Y. Zeng, Y. Zhuge, H. Lu, and L. Zhang, "Joint learning of saliency detection and weakly supervised semantic segmentation," in *Proc. IEEE Int. Conf. Comput. Vis.*, 2019, pp. 7223–7233.
- [104] G. Li and Y. Yu, "Deep contrast learning for salient object detection," in *Proc. IEEE Conf. Comput. Vis. Pattern Recognit.*, 2016, pp. 478–487.
- [105] Y. Tang and X. Wu, "Saliency detection via combining region-level and pixel-level predictions with cnns," in *Proc. Eur. Conf. Comput. Vis.*, 2016, pp. 809–825.
- [106] P. Krähenbühl and V. Koltun, "Efficient inference in fully connected crfs with gaussian edge potentials," in *Proc. Advances Neural Inf. Process. Syst.*, 2011, pp. 109–117.
- [107] M.-M. Cheng, N. J. Mitra, X. Huang, P. H. S. Torr, and S.-M. Hu, "Global contrast based salient region detection," *IEEE Trans. Pattern Anal. Mach. Intell.*, vol. 37, no. 3, pp. 569–582, 2015.
- [108] Y. Li, X. Hou, C. Koch, J. M. Rehg, and A. L. Yuille, "The secrets of salient object segmentation," in *Proc. IEEE Conf. Comput. Vis. Pattern Recognit.*, 2014, pp. 280–287.
- [109] R. Ju, Y. Liu, T. Ren, L. Ge, and G. Wu, "Depth-aware salient object detection using anisotropic center-surround difference," *Signal Processing: Image Communication*, vol. 38, pp. 115–126, 2015.
- [110] H. Peng, B. Li, W. Xiong, W. Hu, and R. Ji, "Rgb-d salient object detection: a benchmark and algorithms," in *Proc. Eur. Conf. Comput. Vis.*, 2014, pp. 92–109.
- [111] M. Jiang, S. Huang, J. Duan, and Q. Zhao, "SALICON: Saliency in context," in *Proc. IEEE Conf. Comput. Vis. Pattern Recognit.*, 2015, pp. 1072–1080.
- [112] J. Zhang, S. Ma, M. Sameki, S. Sclaroff, M. Betke, Z. Lin, X. Shen, B. Price, and R. Mech, "Salient object subitizing," in *Proc. IEEE Conf. Comput. Vis. Pattern Recognit.*, 2015, pp. 4045–4054.
- [113] M. Everingham, L. Van Gool, C. K. Williams, J. Winn, and A. Zisserman, "The pascal visual object classes (voc) challenge," *Int. J. Comput. Vis.*, vol. 88, no. 2, pp. 303–338, 2010.
- [114] J. Deng, W. Dong, R. Socher, L.-J. Li, K. Li, and L. Fei-Fei, "Imagenet: A large-scale hierarchical image database," in *Proc. IEEE Conf. Comput. Vis. Pattern Recognit.*, 2009, pp. 248–255.
- [115] T.-Y. Lin, M. Maire, S. Belongie, J. Hays, P. Perona, D. Ramanan, P. Dollár, and C. L. Zitnick, "Microsoft coco: Common objects in context," in *Proc. Eur. Conf. Comput. Vis.*, 2014, pp. 740–755.
- [116] A. Krizhevsky, I. Sutskever, and G. E. Hinton, "Imagenet classification with deep convolutional neural networks," in *Proc. Advances Neural Inf. Process. Syst.*, 2012, pp. 1097–1105.
- [117] J. Long, E. Shelhamer, and T. Darrell, "Fully convolutional networks for semantic segmentation," in *Proc. IEEE Conf. Comput. Vis. Pattern Recognit.*, 2015, pp. 3431–3440.
- [118] S. Xie and Z. Tu, "Holistically-nested edge detection," in *Proc. IEEE Int. Conf. Comput. Vis.*, 2015, pp. 1395–1403.
- [119] O. Ronneberger, P. Fischer, and T. Brox, "U-net: Convolutional networks for biomedical image segmentation," in *International Conference on Medical Image Computing and Computer-Assisted Intervention*, 2015, pp. 234–241.
- [120] J. Yang, B. Price, S. Cohen, H. Lee, and M.-H. Yang, "Object contour detection with a fully convolutional encoder-decoder network," in *Proc. IEEE Conf. Comput. Vis. Pattern Recognit.*, 2016, pp. 193–202.
- [121] J. L. Long, N. Zhang, and T. Darrell, "Do convnets learn correspondence?" in *Proc. Advances Neural Inf. Process. Syst.*, 2014, pp. 1601–1609.
- [122] B. Zhou, A. Khosla, A. Lapedriza, A. Oliva, and A. Torralba, "Learning deep features for discriminative localization," in *Proc. IEEE Conf. Comput. Vis. Pattern Recognit.*, 2016, pp. 2921–2929.
- [123] J. Zhang, S. Sclaroff, Z. Lin, X. Shen, B. Price, and R. Mech, "Minimum barrier salient object detection at 80 fps," in *Proc. IEEE Int. Conf. Comput. Vis.*, 2015, pp. 1404–1412.
- [124] J. Zhang and S. Sclaroff, "Exploiting surroundedness for saliency detection: a boolean map approach," *IEEE Trans. Pattern Anal. Mach. Intell.*, no. 5, pp. 889–902, 2016.
- [125] R. Caruana, "Multitask learning," *Machine learning*, vol. 28, no. 1, pp. 41–75, 1997.
- [126] E. L. Kaufman, M. W. Lord, T. W. Reese, and J. Volkman, "The discrimination of visual number," *The American Journal of Psychology*, vol. 62, no. 4, pp. 498–525, 1949.
- [127] S. Alpert, M. Galun, R. Basri, and A. Brandt, "Image segmentation by probabilistic bottom-up aggregation and cue integration," in *Proc. IEEE Conf. Comput. Vis. Pattern Recognit.*, 2007, pp. 1–8.
- [128] V. Movahedi and J. H. Elder, "Design and perceptual validation of performance measures for salient object segmentation," in *Proc. IEEE Conf. Comput. Vis. Pattern Recognit. - Workshops*, 2010.
- [129] C. Xia, J. Li, X. Chen, A. Zheng, and Y. Zhang, "What is and what is not a salient object? learning salient object detector by ensembling linear exemplar regressors," in *Proc. IEEE Conf. Comput. Vis. Pattern Recognit.*, 2017, pp. 4321–4329.
- [130] D.-P. Fan, M.-M. Cheng, J.-J. Liu, S.-H. Gao, Q. Hou, and A. Borji, "Salient objects in clutter: Bringing salient object detection to the foreground," in *The Proc. Eur. Conf. Comput. Vis.*, 2018.
- [131] R. Fan, Q. Hou, M.-M. Cheng, G. Yu, R. R. Martin, and S.-M. Hu, "Associating inter-image salient instances for weakly supervised semantic segmentation," in *The Proc. Eur. Conf. Comput. Vis.*, 2018, pp. 367–383.
- [132] J. Zhao, J. Li, H. Liu, S. Yan, and J. Feng, "Fine-grained multi-human parsing," *Int. J. Comput. Vis.*, pp. 1–19, 2019.
- [133] D. Martin, C. Fowlkes, D. Tal, and J. Malik, "A database of human segmented natural images and its application to evaluating segmentation algorithms and measuring ecological statistics," in *Proc. IEEE Int. Conf. Comput. Vis.*, vol. 2, 2001, pp. 416–423.
- [134] J. Xiao, J. Hays, K. A. Ehinger, A. Oliva, and A. Torralba, "Sun database: Large-scale scene recognition from abbey to zoo," in *Proc. IEEE Conf. Comput. Vis. Pattern Recognit.*, 2010, pp. 3485–3492.
- [135] Z. Wang and B. Li, "A two-stage approach to saliency detection in images," in *Proc. IEEE Conf. Acoust. Speech Signal Process.*, 2008, pp. 965–968.
- [136] R. Margolin, L. Zelnik-Manor, and A. Tal, "How to evaluate foreground maps?" in *Proc. IEEE Conf. Comput. Vis. Pattern Recognit.*, 2014, pp. 248–255.
- [137] D.-P. Fan, M.-M. Cheng, Y. Liu, T. Li, and A. Borji, "Structure-measure: A new way to evaluate foreground maps," in *Proc. IEEE Int. Conf. Comput. Vis.*, 2017.
- [138] D.-P. Fan, M.-M. Cheng, J.-J. Liu, S.-H. Gao, Q. Hou, and A. Borji, "Enhanced-alignment measure for binary foreground map eval-

- uation," in *International Joint Conferences on Artificial Intelligence*, 2018.
- [139] F. Perazzi, J. Pont-Tuset, B. McWilliams, L. Van Gool, M. Gross, and A. Sorkine-Hornung, "A benchmark dataset and evaluation methodology for video object segmentation," in *Proc. IEEE Conf. Comput. Vis. Pattern Recognit.*, 2016, pp. 724–732.
- [140] C. Szegedy, W. Zaremba, I. Sutskever, J. Bruna, D. Erhan, I. Goodfellow, and R. Fergus, "Intriguing properties of neural networks," in *Proc. Int. Conf. Learn. Representations*, 2014.
- [141] C. Li, R. Cong, J. Hou, S. Zhang, Y. Qian, and S. Kwong, "Nested network with two-stream pyramid for salient object detection in optical remote sensing images," *IEEE Trans. Geosci. Remote Sens.*, vol. 57, no. 11, pp. 9156–9166, 2019.
- [142] I. Mehmood, M. Sajjad, W. Ejaz, and S. W. Baik, "Saliency-directed prioritization of visual data in wireless surveillance networks," *Information Fusion*, vol. 24, pp. 16–30, 2015.
- [143] Z. Zhang, S. Fidler, and R. Urtasun, "Instance-level segmentation for autonomous driving with deep densely connected mrfs," in *Proc. IEEE Conf. Comput. Vis. Pattern Recognit.*, 2016, pp. 669–677.
- [144] C. Guo and L. Zhang, "A novel multiresolution spatiotemporal saliency detection model and its applications in image and video compression," *IEEE Trans. Image Process.*, vol. 19, no. 1, pp. 185–198, 2009.
- [145] C. Xie, J. Wang, Z. Zhang, Y. Zhou, L. Xie, and A. Yuille, "Adversarial examples for semantic segmentation and object detection," in *Proc. IEEE Conf. Comput. Vis. Pattern Recognit.*, 2017, pp. 1369–1378.
- [146] A. Fawzi, S.-M. Moosavi-Dezfooli, and P. Frossard, "Robustness of classifiers: from adversarial to random noise," in *Proc. Advances Neural Inf. Process. Syst.*, 2016, pp. 1632–1640.
- [147] N. Papernot, P. McDaniel, and I. Goodfellow, "Transferability in machine learning: from phenomena to black-box attacks using adversarial samples," *arXiv preprint arXiv:1605.07277*, 2016.
- [148] Y. Liu, X. Chen, C. Liu, and D. Song, "Delving into transferable adversarial examples and black-box attacks," in *Proc. Int. Conf. Learn. Representations*, 2017.
- [149] A. Torralba and A. A. Efros, "Unbiased look at dataset bias," in *Proc. IEEE Conf. Comput. Vis. Pattern Recognit.*, 2011, pp. 1521–1528.
- [150] K. Simonyan and A. Zisserman, "Very deep convolutional networks for large-scale image recognition," in *Proc. Int. Conf. Learn. Representations*, 2015.
- [151] B. Zoph and Q. V. Le, "Neural architecture search with reinforcement learning," in *Proc. Int. Conf. Learn. Representations*, 2017.
- [152] M. Berman, A. Rannen Triki, and M. B. Blaschko, "The lovász-softmax loss: A tractable surrogate for the optimization of the intersection-over-union measure in neural networks," in *Proc. IEEE Conf. Comput. Vis. Pattern Recognit.*, 2018, pp. 4413–4421.
- [153] T.-W. Ke, J.-J. Hwang, Z. Liu, and S. X. Yu, "Adaptive affinity fields for semantic segmentation," in *Proc. Eur. Conf. Comput. Vis.*, 2018, pp. 587–602.
- [154] E. Bengio, P.-L. Bacon, J. Pineau, and D. Precup, "Conditional computation in neural networks for faster models," in *Proc. Int. Conf. Learn. Representations*, 2016.
- [155] A. Veit and S. Belongie, "Convolutional networks with adaptive inference graphs," in *Proc. Eur. Conf. Comput. Vis.*, 2018.
- [156] A. Zlateski, R. Jaroensri, P. Sharma, and F. Durand, "On the importance of label quality for semantic segmentation," in *Proc. IEEE Conf. Comput. Vis. Pattern Recognit.*, 2018.
- [157] M. Jiang, J. Xu, and Q. Zhao, "Saliency in crowd," in *Proc. Eur. Conf. Comput. Vis.*, 2014, pp. 17–32.
- [158] Q. Zheng, J. Jiao, Y. Cao, and R. W. Lau, "Task-driven webpage saliency," in *Proc. Eur. Conf. Comput. Vis.*, 2018, pp. 287–302.
- [159] A. Palazzi, F. Solera, S. Calderara, S. Alletto, and R. Cucchiara, "Learning where to attend like a human driver," in *IEEE Intelligent Vehicles Symposium*, 2017, pp. 920–925.
- [160] A. K. Mishra, Y. Aloimonos, L. F. Cheong, and A. Kassim, "Active visual segmentation," *IEEE Trans. Pattern Anal. Mach. Intell.*, vol. 34, no. 4, pp. 639–653, 2012.
- [161] C. M. Masciocchi, S. Mihalas, D. Parkhurst, and E. Niebur, "Everyone knows what is interesting: Salient locations which should be fixated," *Journal of Vision*, vol. 9, no. 11, pp. 25–25, 2009.
- [162] A. Borji, "What is a salient object? A dataset and a baseline model for salient object detection," *IEEE Trans. Image Process.*, vol. 24, no. 2, pp. 742–756, 2015.
- [163] L. Jing and Y. Tian, "Self-supervised visual feature learning with deep neural networks: A survey," *IEEE Trans. Pattern Anal. Mach. Intell.*, 2020.
- [164] D. Pathak, P. Krahenbuhl, J. Donahue, T. Darrell, and A. A. Efros, "Context encoders: Feature learning by inpainting," in *Proc. IEEE Conf. Comput. Vis. Pattern Recognit.*, 2016, pp. 2536–2544.
- [165] G. Larsson, M. Maire, and G. Shakhnarovich, "Colorization as a proxy task for visual understanding," in *Proc. IEEE Conf. Comput. Vis. Pattern Recognit.*, 2017, pp. 6874–6883.
- [166] M. Caron, P. Bojanowski, A. Joulin, and M. Douze, "Deep clustering for unsupervised learning of visual features," in *Proc. Eur. Conf. Comput. Vis.*, 2018, pp. 132–149.
- [167] C. Bucilua, R. Caruana, and A. Niculescu-Mizil, "Model compression," in *Proceedings of SIGKDD international conference on Knowledge discovery and data mining*, 2006, pp. 535–541.
- [168] G. Hinton, O. Vinyals, and J. Dean, "Distilling the knowledge in a neural network," in *Proc. Advances Neural Inf. Process. Syst. - workshops*, 2014.
- [169] A. Romero, N. Ballas, S. E. Kahou, A. Chassang, C. Gatta, and Y. Bengio, "Fitnets: Hints for thin deep nets," *arXiv preprint arXiv:1412.6550*, 2014.
- [170] G. Chen, W. Choi, X. Yu, T. Han, and M. Chandraker, "Learning efficient object detection models with knowledge distillation," in *Proc. Advances Neural Inf. Process. Syst.*, 2017, pp. 742–751.